ESPOO 2002 VTT RESEARCH NOTES 2136

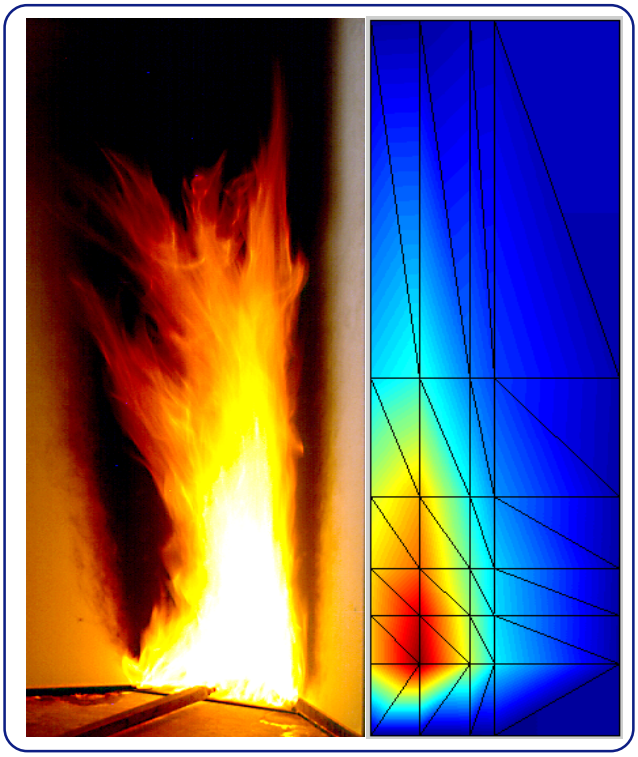

Jukka Hietaniemi & Djebar Baroudi

Physical Interpretation of Temperature Data Measured in the SBI Fire Test

Nordtest Technical Report 416
Nordtest Project No. 1381-98

VTT TIEDOTTEITA – RESEARCH NOTES 2136

Physical Interpretation of Temperature Data Measured in the SBI Fire Test

Nordtest Technical Report 416
Nordtest Project No. 1381-98

Jukka Hietaniemi & Djebar Baroudi
VTT Building and Transport

ISBN 951–38–5958–4 (soft back ed.)
ISSN 1235–0605 (soft back ed.)

ISBN 951–38–5959–2 (URL: http://www.inf.vtt.fi/pdf/)
ISSN 1455–0865 (URL: http://www.inf.vtt.fi/pdf/)

JULKAISIJA – UTGIVARE – PUBLISHER

VTT, Vuorimiehentie 5, PL 2000, 02044 VTT
puh. vaihde (09) 4561, faksi (09) 456 4374

VTT, Bergsmansvägen 5, PB 2000, 02044 VTT
tel. växel (09) 4561, fax (09) 456 4374

VTT Technical Research Centre of Finland, Vuorimiehentie 5, P.O.Box 2000, FIN–02044 VTT, Finland
phone internat. + 358 9 4561, fax + 358 9 456 4374

VTT Rakennus- ja yhdyskuntatekniikka, Kivimiehentie 4, PL 1803, 02044 VTT
puh. vaihde (09) 4561, faksi (09) 456 4815

VTT Bygg och transport, Stenkarlsvägen 4, PB 1803, 02044 VTT
tel. växel (09) 4561, fax (09) 456 4815

VTT Building and Transport, Kivimiehentie 4, P.O.Box 1803, FIN–02044 VTT, Finland
phone internat. + 358 9 4561, fax + 358 9 456 4815

Technical editing Marja Kettunen

Otamedia Oy, Espoo 2002

Hietaniemi Jukka & Baroudi, Djebar. Physical Interpretation of Temperature Data Measured in the SBI Fire Test. Nordtest Technical Report 416. Nordtest Project No. 1381-98. Espoo 2002. VTT Tiedotteita – Research Notes 2136. 47 p. + app. 4 p.

Keywords fire tests, fire protection, SBI, temperature measurement, data analysis, exhaust gases, heat transfer

Abstract

In the SBI fire test, there are temperature sensors in the exhaust duct allowing measurement of the temperature rise of the exhaust gases (ΔT measurement). In principle these sensors provide means to monitor the production rate of thermal energy. However, while traversing to the exhaust duct the heated gases lose energy to their surroundings which in a rigorous determination of the heat release rate of the specimen must be taken into account. There is also another factor hampering the conversion of the ΔT values to the thermal energy readings, namely the fact that the temperature readings do not directly show the temperature of the gases, but rather reflect it through a heat transfer process involving also the duct wall temperatures. These complications make the experimentally simple ΔT approach for rate-of-heat-release evaluation a complex task with inherently high uncertainty and proneness to systematic errors. Thus the method is not suitable for routine testing and classification purposes.

However, for some other applications, such as quality control and product development purposes, the ΔT method can in some cases provide a well-suited option for RHR assessment. The method can also be used in fire research, e.g., to analyse the convective portion of the total heat release.

In this report we present a method to interpret the ΔT values in terms of physically relevant factors describing generation and loss of heat. The analysis yields straightforwardly the convective part of RHR of the specimen. However, to evaluate the total RHR of the specimen, external sources of information must be exploited to establish the radiative contribution of the total RHR.

The analysis method is based on a simplified model of heat transfer in the SBI system and its mathematical formulation. The solution of the problem entails handling of an inverse heat-transfer problem. The novelty of the presented solution lies in the use of the regularised output least-squares method to tackle with this problem. The dextrous numerical solution of developed enables execution of the whole analysis by a spreadsheet program (EXCEL). As majority of the operations can be executed automatically by EXCEL Macros, integration of the program into, e.g., the SBI data-analysis software is straightforward.

Experiments were carried out to establish and verify the heat transfer model and to check the operation of the calculation codes.

Besides the use in connection with the SBI apparatus, the data analysis method developed in this study can in principle be applied also in other fire tests.

Preface

According to the decisions of the European Commission in 1994 and 2000, the reaction-to-fire behaviour of construction products will be classified with the Euroclass system. The test method scheme of the Euroclass system relies strongly on the Single-Burning Item (SBI) test, which will be used for testing building products other than floors.

The measurement of the rate of heat release (RHR) of the specimen in the SBI test is based on the well-established oxygen-depletion principle. In the early development phases of the method also the possibility to evaluate the RHR via temperature measurements of the exhaust gases was considered but because of obvious reasons related to measurement precision and trueness this method was dropped. However, the temperature sensors intended for the exhaust gas temperature change measurements (ΔT measurements) are still a part of the SBI apparatus. Thus, they could be utilised, e.g., in quality control and product development work carried out by an SBI apparatus as well as for research purposes.

In this study, an analysis method is established for evaluating the convective part of the rate of heat release from the temperature readings. The method is based on modelling the principal heat transfer properties of the system and giving the model a rigid mathematical formulation. The solution of the system is implemented in an easy-to-use, compact spreadsheet code.

The work was carried out as a Nordtest Project no. 1381-98 with funding from Nordtest and VTT Building and Transport.

Contents

List of symbols

Symbol	Meaning
T_{meas}	temperature measured in the temperature-measurement section of the duct (K)
T_{gas}	temperature of the gas flowing in the duct at the temperature-measurement section (K)
T_{in}	temperature of the inner wall of the duct at the temperature-measurement section (K)
T_0	initial temperature of the system (K)
$T_{\infty,conv}$	ambient temperature for convective heat transfer at the out surface of the duct (K)
$T_{\infty,rad}$	ambient temperature for radiative heat transfer at the out surface of the duct (K)
$T_{s,1}$	temperature of the inner metal sheet (K)
$T_{s,2}$	temperature of the outer metal sheet (K)
T_i	temperature of the insulator of the duct (associated to the heat transfer through the duct wall) (K)
C_{ins}	specific heat of the insulator of the duct ($J \cdot kg^{-1} \cdot K^{-1}$)
k_{ins}	thermal conductivity of the insulator of the duct ($W \cdot m^{-1} \cdot K^{-1}$)
ρ_{ins}	density of the insulator of the duct ($kg \cdot m^{-3}$)
$\kappa_{ins} = k_{ins} / \left(\rho_{ins} C_{ins} \right)$	thermal diffusivity of the of the duct ($m^2 s^{-1}$)
C_s	specific heat of the steel plates of the duct ($J \cdot kg^{-1} \cdot K^{-1}$)
ρ_s	density of the steel plates of the duct ($kg \cdot m^{-3}$)
d_s	thickness of the metal sheets (m)
d_i	thickness of the insulator (m)
$A_{s,1}^{(in)} = 2\pi R_{in} L_{duct}$	area of heat transfer of the inner face of the inner metal sheet (m^2)

$A_{s,1}^{(out)} = 2\pi\left(R_{in} + d_s\right)L_{duct}$ $\approx 2\pi R_{in} L_{duct} = A_{s,1}^{(in)}$	area of heat transfer of the outer face of the inner metal sheet (m^2)
$A_{s,2}^{(in)} = 2\pi\left(R_{in} + d_s + d_i\right)L_{duct}$ $\approx 2\pi\left(R_{in} + d_{in}\right)L_{duct}$	area of heat transfer of the inner face of the outer metal sheet (m^2)
$A_{s,2}^{(out)} = 2\pi\left(R_{in} + 2d_s + d_i\right)L_{duct}$ $\approx 2\pi\left(R_{in} + d_{in}\right)L_{duct} = A_{s,2}^{(in)}$	area of heat transfer of the outer face of the outer metal sheet (m^2)
$V_{s,1} = \pi\left[\left(R_{in} + d_s\right)^2 - R_{in}^2\right]L_{duct}$ $\approx 2\pi R_{in} d_s L_{duct}$	volume of the inner and outer metal sheets (m^3)
$V_{s,2} = \pi\left[\left(R_{in} + 2d_s + d_i\right)^2 - \left(R_{in} + d_s + d_i\right)^2\right]L_{duct}$ $\approx 2\pi\left(R_{in} + d_i\right)d_s L_{duct}$	volume of the insulator (m^3)
h_{in}	heat transfer coefficient of the inner wall of the duct ($W \cdot m^{-2} \cdot K^{-1}$)
h_{out}	heat transfer coefficient of the outer wall of the duct ($W \cdot m^{-2} \cdot K^{-1}$)
t	time (s)
r	radial co-ordinate (m)
C_c	specific heat of the temperature sensor ($J \cdot kg^{-1} \cdot K^{-1}$)
h_c	heat transfer coefficient of the temperature sensor ($W \cdot m^{-2} \cdot K^{-1}$)
ρ_c	density of the temperature sensor ($kg \cdot m^{-3}$)
$V_c = (4\pi/3)r_c^3$	volume of the temperature sensor (m^3)
$A_c = 4\pi r_c^2$	surface area of the temperature sensor (m^2)
r_c	radius of the temperature sensor (m)
ε_c	emissivity of the temperature sensor (-)
ε_{gas}	emissivity of the gas in the duct (-)
ε_{in}	emissivity of the inner wall of the duct (-)

ε_{out}	emissivity of the outer wall of the duct (-)
ϕ_{cg}	radiation configuration factor between the gas and the sensor (set equal to unity) (-)
ϕ_{cw}	radiation configuration factor between the inner wall of the and the sensor, approximately $L_{duct} \Big/ \sqrt{L_{duct}^2 + R_{in}^2} \approx 1$ (-)
f_T	factor describing the transmittance of the radiation from the inner duct wall to the temperature sensor through the gas: no transmittance $f_T = 1$ and full transmittance $f_T = 0$ (-)
L_{duct}	length of the section of the duct associated with heat-transfer problem (m)
R_{in}	radius of the inner wall of the duct (m)
σ	Stefan-Boltzman constant ($5.67 \cdot 10^{-8}$ W·m^{-2}·K^{-4})

1. Introduction

According to the decisions of the European Commission in 1994 and 2000, the reaction-to-fire behaviour of construction products used in ceilings and walls will be classified with the Euroclass system. The Single-Burning Item (SBI) test is an important Euroclass test method.

The measurement of the rate of heat release (RHR) of the specimen in the SBI test is based on the well-established oxygen-depletion principle [Parker 1984]. However, in the early phases of the SBI development work, the measurement of the temperature rise of the exhaust gases, or, in short, the ΔT measurement, was considered as a possible option the obtain a quantity reflecting the heat released of the specimen.

As the oxygen-depletion technique for RHR evaluation requires precise analysis of the exhaust gas O_2 and CO_2 concentrations, it may be considered as an experimentally elaborate method. However, practise has proven that the technique is an accurate and repeatable method suitable for routine fire testing. Using ΔT measurements to gauge the RHR value is experimentally simple technique. However, with respect to data analysis it is a very complex method, as rigorous interpretation of the ΔT value in terms of the heat release requires knowledge of the thermal response of the whole system. This gives rise to high uncertainty in the results obtained, both stochastic and systematic. Together with the fact that temperature readings can only reveal the convective part of the RHR, it is clear that the ΔT measurement method is not suitable for testing and classification purposes.

However, for less demanding applications, such as quality control and product development purposes the ΔT can in some cases provide a well-suited option for RHR assessment. The method can also be used in fire research, e.g., to analyse the convective portion of the total heat release.

This study addresses the problem of interpreting the ΔT values in terms of physically relevant quantities such as the rate of heat release. The analysis produces straightforwardly the convective part of RHR of the specimen. To elaborate the results further in order to get an estimate of the total heat released, additional information is required on the partitioning of the RHR to its convective and radiative portions. The method developed in this study is based on a simplified model of the heat transfer in the SBI system and a mathematical formulation to describe this system. Experiments were carried out to check the operation of the calculation codes and to establish and verify the heat transfer model.

The solution of the problem entails handling of an inverse heat-transfer problem. The novelty of the presented solution lies in the use of the regularised output least-squares method to tackle with this problem. The dextrous numerical solution of developed enables execution of the whole analysis by a spreadsheet program (EXCEL). As majority of the operations can be executed automatically by EXCEL Macros, integration of the program into, e.g., the SBI data-analysis software is straightforward.

The analysis of the ΔT data has been broken to four tasks, each of which is executed by a separate EXCEL workbook. These tasks are: 1) data retrieval from the SBI data files and their pre-processing, 2) solving the heat flow rate in the exhaust duct from the ΔT data, 3) calculations to predict the major heat loss terms and 4) combination of the results to the final results.

Besides the use in connection with the SBI apparatus, the data analysis method developed in this study can in principle be applied also in other fire tests.

First, in Chapter 2, some basic properties of the SBI apparatus are presented and then the model to describe the heat transfer in the system is developed. In Chapter 3, the mathematical details of the heat transfer problems are formulated together with presentations of the solution techniques. Evaluation of the heat loss terms is presented in Chapter 4. In Chapter 5 we present results obtained by applying the analysis to some tests performed in the SBI Round Robin. Summary and some concluding remarks are given in Chapter 6.

2. The SBI apparatus and a model for the heat transfer in the system

2.1 The SBI test: apparatus and procedure

The SBI fire test simulates the thermal attack from a single burning item located in a corner between two walls made of the tested product. The rate of production of heat and smoke by the specimen are derived from quantities measured in the exhaust duct. The principal features of the SBI apparatus are shown in Figure 1a.

The heat exposure simulating the burning item is produced by a burner placed in the corner (see Figure 1b). This burner is called the main burner. It is on through the whole test. There is also another burner in the system, the auxiliary burner, which is operated for the first three minutes before the actual test (see Figure 1c). Then, the auxiliary burner is switched off and the main burner is ignited. Thereafter the main burner is allowed to burn for 1200 s, which constitutes the actual SBI test interval. The nominal burner heat output level is 30 kW for the both burners. For the first two minutes of the test, the data acquisition devices collect base line data.

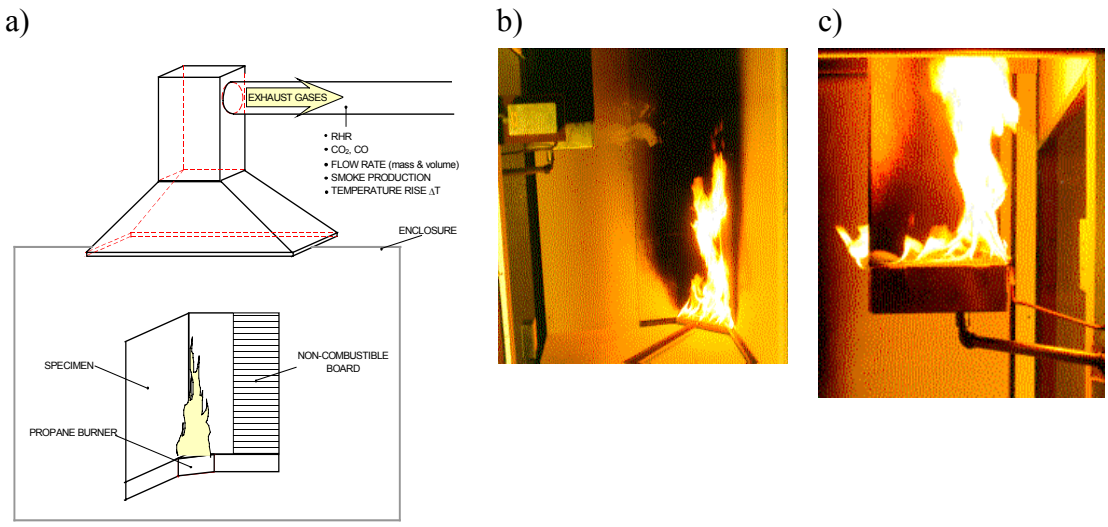

Figure 1. a) A schematic figure showing the principal features of the SBI apparatus, b) photograph showing the corner configuration with the main burner and c) the auxiliary burner.

The temperature measurements in the SBI test are performed in two locations of the duct, at the beginning of the duct (temperature measurement section, TMS) and further downstream (general measurement section, GMS). The former readings are used in the temperature rise measurements whereas the latter measurements are used as auxiliary quantities for the duct flow rate evaluation.

The specimen and the burner are located in an enclosed space to reduce influence of external factors such as air currents and also to enhance the comfort and safety of the operator of the system. The SBI set up of VTT Building and Transport is shown in Figure 2.

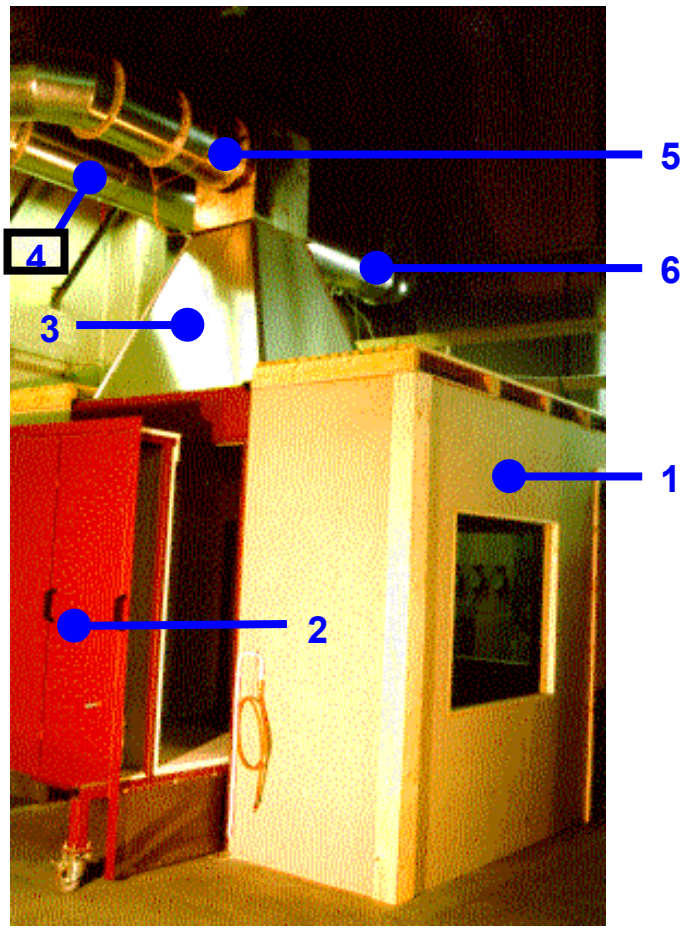

1. Enclosure
2. Trolley
3. Exhaust collection hood
4. Exhaust duct
5. Temperature measurement section (TMS)
6. General measurement section (GMS)

Figure 2. A photograph of the SBI apparatus showing the cabin enclosing the actual test space, the trolley used to transfer the specimens to the test space, the exhaust hood and the exhaust duct. The measuring sensors in the duct are placed at the two positions depicted in the photo, the position close to the duct beginning is called the temperature measurement section (TMS) and the other at position further downstream is called the general measurement section (GMS).

2.2 Conversion of the measure temperatures to convective heat release rate of the specimen

The data from which the convected heat release rate of the specimen is deduced are measured temperatures at the temperature measurement section of the system. We refer to this measure, obtained as an average of several thermocouple readings, as T_c.

This temperature is related to the temperature of the gases flowing in duct, T_{gas}, through the convective and radiative heat transfer which is elaborated in details in Chapter 3.

The values of T_{gas} may be used to calculate the enthalpy flow rate in the duct which in a constant pressure system like the SBI apparatus equals the heat flow rate:

$$\dot{Q}_{gas} = C_{p,gas}\rho_{gas}\dot{V}_{duct}\Delta T_{gas} \quad (2.1)$$

Here, ΔT_{gas} is the rise of the gas temperature above its initial value, $C_{p,gas}$ is the specific heat of the exhaust gases (taken here to be equal to that of air at 298 K), ρ_{gas} is the density of the exhaust gases (taken here to be equal to that of air at the T_{gas}) and $\dot{V}_{duct}$ is the flow rate in the exhaust duct.

The heat flowing in the exhaust duct during the SBI test embodies two contributions, that originating from the heat released by the specimen, $\dot{Q}_{gas,specimen}$, and that coming from the main burner, $\dot{Q}_{gas,main}$, *i.e.*,

$$\dot{Q}_{gas} = \dot{Q}_{gas,specimen} + \dot{Q}_{gas,main} \quad (2.2)$$

To convert the contribution of the specimen to the duct gas heat flow to the convective fraction of the heat released by the specimen $\dot{Q}_{conv,specimen}$, various heat loss terms, collective denoted as $\dot{Q}_{loss,specimen}$, must be taken into account. Also the main burner contribution to the duct heat flow differs from the heat generated by the burner by losses occurring while the gases flow from the burner to the duct.

$$\dot{Q}_{gas,specimen} = \dot{Q}_{conv,specimen} - \dot{Q}_{loss,specimen} \quad (2.3a)$$

and

$$\dot{Q}_{gas,main} = \dot{Q}_{conv,main} - \dot{Q}_{loss,main} \quad (2.3b)$$

Thus, the convective fraction of the heat released by the specimen which is the primary output of the calculations reads

$$\dot{Q}_{conv,specimen} = \dot{Q}_{gas} + \dot{Q}_{loss,specimen} - \left(\dot{Q}_{conv,main} - \dot{Q}_{loss,main}\right) \quad (2.4)$$

The different mechanisms included in the heat loss terms of Eq. (2.4) are considered below.

2.3 Model for the heat transfer in the system

The complete heat transfer scheme of the SBI system is very complex and to enable any practical computational approach, several simplifying assumptions must be introduced. The simplifications employed in this study to model the heat transfer in the SBI system are presented in Figure 3. The model takes into account the following heat losses that constitute the major portion of all the losses in the system. The dominant factor is the radiation from the flames and next in importance are the losses arising from direct contact of the flames or the hot gases to the surfaces in the system.

In the present study, no attempts are made to quantify the radiation losses since there are no radiation measurements in the basic SBI test set up. Radiative heat transfer is, however, considered in the equations describing the heat transfer to the duct wall or from the main burner to the specimen.

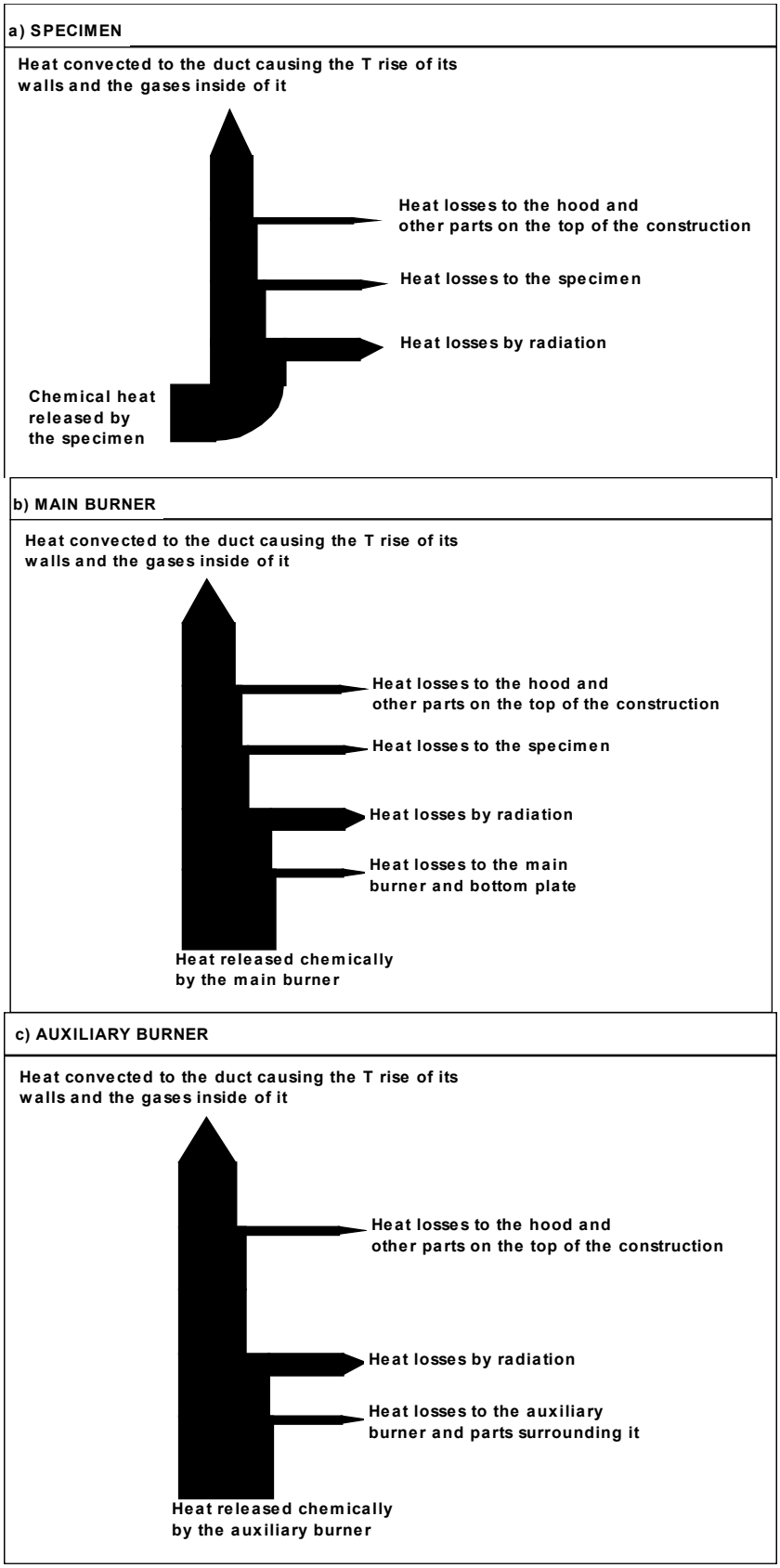

Figure 3. Components of the heat transfer system included in the model: the heat originating from the specimen (a), the heat from the main burner (b) and the heat from the auxiliary burner (c).

2.3.1 Heat generated by the specimen and the associated losses

The heat produced by the specimen may be analysed in terms of the following quotients:

- The chemical heat production by the specimen $\dot{Q}_{chem,specimen}$.
- The losses due to radiation $\dot{Q}_{rad,specimen}$.
- The convective fraction $\dot{Q}_{conv,specimen}$ of the specimen's heat generation rate.

The quantity $\dot{Q}_{chem,specimen}$ is the heat released by the specimen, referred to in the SBI nomenclature as RHR_{sample}.

The relation between the above factors is

$$\dot{Q}_{chem,specimen} = \dot{Q}_{rad,specimen} + \dot{Q}_{conv,specimen}, \tag{2.5}$$

which expressed in terms of the convective fraction characterising the particular specimen material $\chi_{conv} = \chi_{chem} - \chi_{rad}$, reads

$$\dot{Q}_{conv,specimen} = \chi_{conv}\ \dot{Q}_{chem,specimen}, \tag{2.6}$$

where χ_{chem} and χ_{rad} are the fractions of chemical and radiative heat release, respectively.

The portion $\dot{Q}_{conv,specimen}$ of the heat is convected along with the flames and the plume and ultimately enters the exhaust duct. The heat losses associated with $\dot{Q}_{conv,specimen}$ may be broken down to those due to the absorption of heat back to the specimen itself, $\dot{Q}_{loss,sa,specimen}$, and those occurring in the exhaust collection hood and other constructions residing in the upper part of the system, collectively referred to by a symbol $\dot{Q}_{loss,hood,specimen}$. The measuring devices in the SBI apparatus provide no direct means to infer either of these heat loss terms. Also estimates for them using theoretical modelling are beyond the scope of the present study. As the temperatures at the upper parts of the system and the hood are much lower than those encountered closer to fires, the loss term $\dot{Q}_{loss,hood,specimen}$ may be assumed to be small and, thus, may be omitted. The magnitude of

the term $\dot{Q}_{loss,sa,specimen}$ is assumed to be 10 percent[†] of the heat convected from the sample.

Summarising the above considerations, we may express the losses associated with the convective fraction of the heat release of the specimen as

$$\dot{Q}_{loss,specimen} \approx \left(\frac{10}{100}\right)\dot{Q}_{conv,specimen} . \tag{2.7}$$

2.3.2 Heat generated by the burners

The heat generated by the burners is calculated as

$$\dot{Q}_{chem,burner} = \chi_{chem,propane}\ \Delta H_{c,propane}\ \dot{m}_{burner} , \tag{2.8}$$

where $\Delta H_{c,propane} = 46$ MJ/kg [Babrauskas 1997] is the net heat of combustion of propane, $\chi_{chem,propane} = 95$ % [Tewarson 1995] is the fraction of chemical heat release and $\dot{m}_{burner}$ is the propane consumption rate of the burner. In the SBI test, the propane feeding rate should be $\dot{m}_{burner} = 647 \pm 10$ mg/s and thus, nominally the heat released by the main and auxiliary burners is $\dot{Q}_{chem,burner} = \dot{Q}_{chem,main} = \dot{Q}_{chem,aux} = 28.5 \pm 0.5$ kW. For the sake of exactitude, in the actual data analysis the measured values of the burner propane mass flow rates were used instead of the nominal values.

The heat produced by the burners may be broken down to radiative and convective portions analogously to Eqs. (2.5) and (2.6). For the convective and radiative fraction of propane we use the following values [Tewarson 1995]: $\chi_{conv,propane} = 68$ % and $\chi_{rad,propane} = 27$ %. Using the above values for $\Delta H_{c,propane}$ and $\dot{m}_{burner}$, the nominal convective and radiative portions of the burner heat release are 20.4 kW and 8.1 kW, respectively.

The loss factors associated with the convective portion of the burner heat release considered in this study are the following: losses to the burner and materials surrounding it, losses to the specimen and losses to the hood and other upper-part constructions. The heat generation and loss terms of the two burners are summarised in Table 1.

[†] Motivation for using the value of 10 % may be found in Chapter 4.

In the data reduction, we are mainly interest in quantifying the main burner properties. The usage of the auxiliary burner data is to predict the main burner properties.

The heat losses associated with the two burners are not, however, identical as the main burner is in direct contact to the bottom plate and its flames sweep the surface of the specimen. For the auxiliary burner such losses do not exist. The loss terms which may be considered to be equal for the two burners are the losses to the hood and to upper construction parts of the apparatus. Also the losses to the burners themselves are roughly equal.

In the analysis of the main burner contribution, the principal convective loss component is the heat transfer to the specimen. The magnitude of this loss term was deduced from calculations and verified by measurements. The other heat losses, *i.e.*, those arising from heat transfer to the burner and materials surrounding it and to the hood and other constructions in the upper part of the SBI system, are treated as a lumped quantity which may be obtained from the auxiliary burner data.

Thus, we may summarise the heat generation and loss terms needed in Eq. (2.4) as

$$\dot{Q}_{conv,main} - \dot{Q}_{loss,main} = \chi_{conv} \Delta H_{c,propane} \dot{m}_{burner} - \left(\dot{Q}_{loss,specimen,main} + \dot{Q}_{loss,other,main} \right) . \qquad (2.9)$$

The last term on the right-hand side of Eq. (2.9) is evaluated through the assumption that this loss term is the same for the main burner and the auxiliary burner. For the auxiliary burner this term is assumed to be the only non-negligible loss associated with convective heat transfer. Thus, it may obtained in straightforward way by comparing the convective heat coming from the burner and the heat flow rate in the exhaust duct during the initial period of the test when the only the auxiliary burner is on. The term $\dot{Q}_{loss,specimen,main}$ is determined by calculations, the validity of which was verified empirically as described in Chapter 4.

Table 1. Heat loss terms associated with the heat released by the burners.

quantity	**main burner**	**auxiliary burner**	**note on evaluation**
chemical heat release	$\dot{Q}_{chem,main}$	$\dot{Q}_{chem,aux}$	Eq. (2.3)
heat loss to the burner and materials in its vicinity	$\dot{Q}_{loss,sa,main}$	$\dot{Q}_{loss,sa,aux}$	$\dot{Q}_{loss,sa,main} \approx \dot{Q}_{loss,sa,aux}$, obtained from aux. burner data, treated lumped to term $\dot{Q}_{loss,other,main}$ with the losses to the hood and other upper part constructions
heat loss to the specimen	$\dot{Q}_{loss,spec,main}$	$\dot{Q}_{loss,spec,aux}$	$\dot{Q}_{loss,spec,main}$, calculated (see Ch. 4) $\dot{Q}_{loss,spec,aux} = 0$
heat loss to the hood and other upper part constructions	$\dot{Q}_{loss,hood,main}$	$\dot{Q}_{loss,hood,aux}$	$\dot{Q}_{loss,hood,main} \approx \dot{Q}_{loss,hood,aux}$, obtained from aux. burner data, treated lumped to term $\dot{Q}_{loss,other,main}$ with the losses to the burner and materials in its vicinity
	$\dot{Q}_{loss,rad,main}$	$\dot{Q}_{loss,rad,aux}$	$\dot{Q}_{loss,rad,main} \approx \dot{Q}_{loss,rad,aux}$, taken into account by radiative fraction of propane $\chi_{rad,propane} = 27\ \%$

3. Detailed mathematical formulation

To utilise the model described in Chapter 2, one must determine the heat flow rate in the exhaust duct. This requires evaluation of how the measured temperature and the temperature of the gases are related, *i.e.*, solving the non-linear ordinary differential equation (3.1). The gas-thermocouple heat transfer system is affected also by the heat transfer through the duct wall, which involves solving a partial differential equation. The formulation of these problems and their solutions are described in sections 3.1 and 3.2.

If the non-linearities could be omitted, the system could be analysed using the powerful transfer function techniques based on the Laplace transform approach (see e.g. [Vandevelde 1980]). However, in the present system the non-linearities arising from the heat transfer through the duct wall are unavoidably present and also the non-linear radiation terms can not neglected at elevated temperatures which may frequently be encountered in SBI test.

Solution of the gas temperature using the values measured with thermocouples means that one has to solve an inverse problem, *i.e.*, to find out what is the cause when the effect is known. Heat transfer problems are difficult solve inversely since a single effect may be a result of many different causes. Mathematically this means that the inverse problem is ill-posed and, thus, to find a meaningful solution to it one must use additional information of the system (*e.g.* some constraints). This process, regularisation, is covered in section 3.3.

3.1 Heat-transfer problem of the measured temperature

Let us consider the set-up shown schematically in Figure 4, which incorporates the main features of the SBI temperature measurement system. The measured temperature T_{meas} depends on the temperature of the gas flowing in the duct, T_{gas}, and the temperature of the inner face of the duct wall, T_{in}, as

$$\rho_c V_c C_c \frac{\mathrm{d}T_{meas}}{\mathrm{d}t} = A_c h_c \left(T_{gas} - T_{meas} \right) - \varepsilon_c A_c \sigma T_{meas}^4 + \left(1 - f_T\right) \phi_{cw} \varepsilon_{in} A_c \sigma T_{in}^4 + + f_T \phi_{cg} \varepsilon_{gas} A_c \sigma T_{gas}^4 , \quad (3.1)$$

where ρ_c, V_c, C_c, A_c and h_c are the density, volume, specific heat, surface area and heat transfer coefficient of the temperature sensor, respectively. For a spherical sensor with a radius r_c, the volume and area are $V_c = \left(4\pi/3\right) r_c^3$ and $A_c = 4\pi r_c^2$. The Stefan-Boltzman constant is $\sigma = 5.67 \cdot 10^{-8}\,\mathrm{kWm^{-2}K^{-4}}$. The emissivities of the inner wall of the duct, the temperature sensor and the gas are ε_{in}, ε_c and ε_{gas}, respectively. The configuration factor for radiation between the gas and the sensor $\phi_{cg} = 1$ has been shown explicitly. The

configuration factor for radiative energy exchange between the duct wall and the sensor ϕ_{cw} [†] is close to unity. For completeness we have included also a factor f_T that takes into account the loss of the heat radiation while it traverses the gas. This factor is assigned a value of $f_T = 0$, *i.e.*, no losses are taken into account.

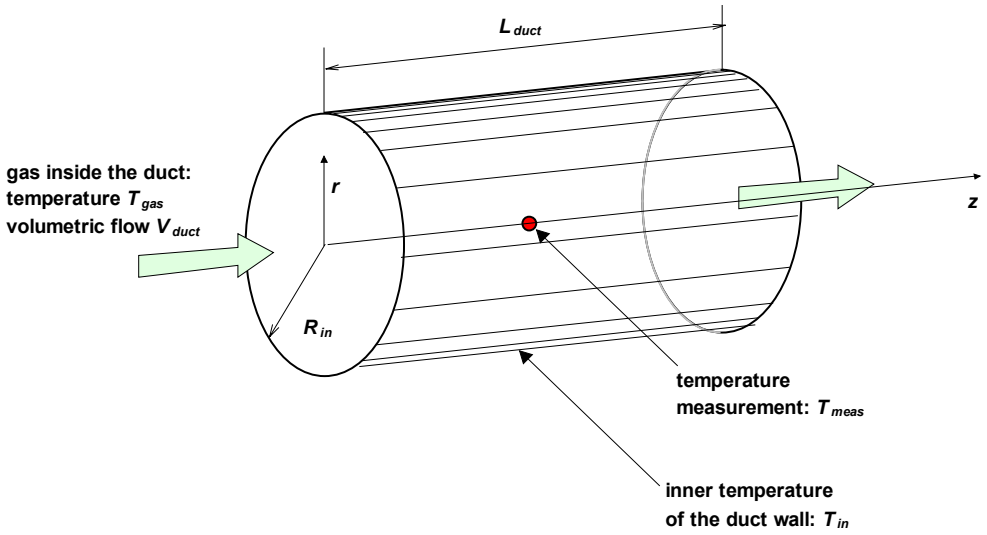

Figure 4. Schematic representation of the temperature measurement system of the SBI fire test apparatus.

Relation (3.1) depicts that, initially, as the duct wall is considerably colder than the gas and the temperature sensor, the measured temperature is lowered from the gas temperature by the radiative losses to the duct wall. As the wall during the test gradually becomes warmer, the radiative losses decrease, and the measured temperature approaches the gas temperature.

[†] For a sensor located in the centre of the duct, the configuration factor is $\phi_{cw} = L_{duct} \Big/ \sqrt{L_{duct}^2 + R_{in}^2} \approx 1$ when $L_{duct} >> R_{duct}$.

3.2 Heat transfer through the duct wall

3.2.1 Formulation of the problem

To utilise Eq. (3.1) to predict the relation between the gas temperature and the measured temperature, we must evaluate the temperature of the inner wall of the duct. This may be accomplished by solving the heat-transfer equations for the system in shown in Figure 5. In this system, heat is transferred from the gas in the duct to the ambient atmosphere surrounding the duct through the duct wall consisting of an insulating layer sandwiched between two metal sheets. The temperature of the inner face of the duct wall required in Eq. (3.1) is the temperature of the inner metal sheet:

$$T_{in} = T_{s,1}\,. \tag{3.2}$$

In the analysis, we will employ the assumptions of the temperature distribution, schematically depicted in the upper part of Figure 5, *i.e.*, in the well-conducting metal plates there is no temperature gradient, and, besides in the thin boundary layers, the temperatures of the gases are constant with respect to spatial dimensions.

The differential equation governing the heat transfer in the insulating layer reads

$$\frac{\partial T_{ins}}{\partial t} = \kappa_{ins}\left(\frac{\partial^2 T_{ins}}{\partial r^2} + \frac{1}{r}\frac{\partial T_{ins}}{\partial r}\right)\,, \tag{3.3a}$$

where T_{ins} is the insulator temperature and

$$\kappa_{ins} = \frac{k_{ins}}{\rho_{ins} C_{ins}} \tag{3.3b}$$

is the thermal diffusivity of the insulator material, with k_{ins}, ρ_{ins} and C_{ins} denoting the thermal conductivity, density and the specific heat of the insulator.

The boundary conditions at $r = d_s$ and $r = d_i + d_s$ may be expressed in terms of the changes in the internal energies of the steel plates as:

$$\rho_s V_{s,1} C_s \frac{\mathrm{d}T_{s,1}}{\mathrm{d}t} = A_{s,1}^{(in)} h_{in}\left(T_{gas} - T_{s,1}\right) - \left(-A_{s,1}^{(out)} k_i \frac{\partial T_{ins}}{\partial r}\right), \text{ at } r = d_s \tag{3.4a}$$

and

$$\rho_s V_{s,2} C_s \frac{\mathrm{d}T_{s,2}}{\mathrm{d}t} = \left(- A_{s,2}^{(in)} k_i \frac{\partial T_{ins}}{\partial r} \right) - \\ - A_{s,2}^{(out)} h_{out} \left(T_{s,1} - T_{\infty,conv} \right) - A_{s,2}^{(out)} \sigma \varepsilon_{out} \left(T_{s,2}^4 - T_{\infty,rad}^4 \right) \quad \text{,at } r = d_i + d_s \,. \tag{3.4b}$$

Here, k_s, ρ_s and C_s denote the thermal conductivity, density and the specific heat of the metal sheets which are at temperatures $T_{s,1}$ an $T_{s,2}$, with 1 referring to the inner sheet and 2 referring to the outer sheet. The heat transfer coefficients at the inner and outer sheets are h_{in} and h_{out}, respectively. Convection of heat takes place to an ambient temperature $T_{\infty,conv}$. For completeness we have included in Eq. (3.4b) the radiative losses from the outer duct face to surrounding surfaces at the ambient temperature $T_{\infty,rad}$. The quantities $V_{s,j}$ (j = 1,2) denote the volumes of the metal sheets:

$$V_{s,1} = \pi \left[\left(R_{in} + d_s \right)^2 - R_{in}^2 \right] L_{duct} \approx 2\pi R_{in} d_s L_{duct} \tag{3.5a}$$

and

$$V_{s,2} = \pi \left[\left(R_{in} + 2d_s + d_i \right)^2 - \left(R_{in} + d_s + d_i \right)^2 \right] L_{duct} \approx 2\pi \left(R_{in} + d_i \right) d_s L_{duct} \tag{3.5b}$$

where R_{in} is the inner radius of the duct, d_s is the thickness of the metal sheets and d_i the thickness of the insulator. The heat-exchange areas on the inner and outer faces of the metal sheets $A_{s,j}^{(in)}$ and $A_{s,j}^{(out)}$ (j = 1,2) are

$$A_{s,1}^{(in)} = 2\pi R_{in} L_{duct} \,, \tag{3.6a}$$

$$A_{s,1}^{(out)} = 2\pi \left(R_{in} + d_s \right) L_{duct} \approx 2\pi R_{in} L_{duct} = A_{s,1}^{(in)} \,, \tag{3.6b}$$

$$A_{s,2}^{(in)} = 2\pi \left(R_{in} + d_s + d_i \right) L_{duct} \approx 2\pi \left(R_{in} + d_i \right) L_{duct} \,, \tag{3.6c}$$

and

$$A_{s,2}^{(out)} = 2\pi \left(R_{in} + 2d_s + d_i \right) L_{duct} \approx 2\pi \left(R_{in} + d_i \right) L_{duct} = A_{s,2}^{(in)} \,, \tag{3.6d}$$

where simplifying approximations, valid for the thin metal sheets are used.

For the gas in the duct, the initial condition may be expressed as

$$T_{gas} = T_0 \quad \text{, when } -\infty < t < 0 \,, \tag{3.7}$$

whereas after the test is started (t > 0),

$$T_{gas} = T_0 + \Delta T_{gas} \quad \text{, when } t \geq 0 \,. \tag{3.8}$$

where the temperature rise ΔT_{gas} depends on the heat released by the burner and specimen as explained in Chapter 2 and T_0 is the initial temperature of the system. Frequently T_0 equals the ambient T_∞, but not necessarily. For the metal sheets and the insulating material, the initial conditions are

$$T_{gs,1} = T_{gs,2} = T_i = T_0 \quad \text{, when } -\infty < t \leq 0 \,. \tag{3.9}$$

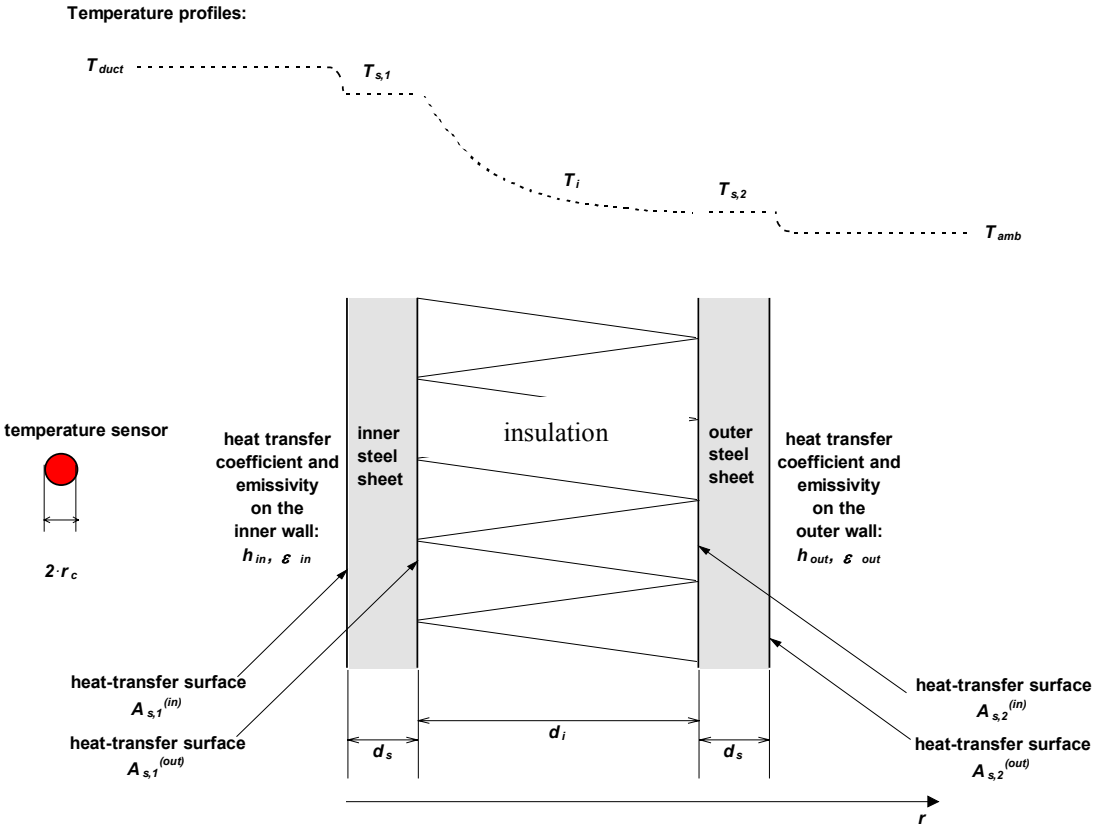

Figure 5. Arrangement of the heat-transfer problem.

3.2.2 Numerical solution of the problem

The major mathematical problem associated with the heat transfer in the above described system is that of the heat conduction through the duct wall or, more specifically, through the insulator of the duct wall as the thin metal sheets may be considered as lumped heat capacity systems.

To facilitate the description of the numerical solution of the heat conduction through the duct wall, we recapitulate the differential equation of the heat conduction problem is as follow: the spatial distribution and temporal evolution of the insulator temperature is described by the differential equation

$$\rho_{ins} C_{ins} \frac{\partial T_{ins}}{\partial t} = -\nabla \cdot \dot{\mathbf{q}}'' \tag{3.10}$$

together with the Fourier's constitutive equation relating the heat flux $\mathbf{q}''$ to the temperature of the insulator as

$$\dot{\mathbf{q}}'' = -k_{ins} \nabla T_{ins} . \tag{3.11}$$

For numerical calculation purposes the above differential formulation may be transformed to the following integral formulation

$$\int_{\Omega} \rho_{ins} C_{ins} \frac{\partial T_{ins}}{\partial t} v \; d\Omega + \int_{\Omega} k_{ins} \nabla T_{ins} \cdot \nabla v \; d\Omega = -\int_{\Gamma} \mathbf{q}'' \cdot \mathbf{n} \, v \; d\Gamma \tag{3.12}$$

which is obtained by multiplying the differential equation by a function v and integrating over the volume Ω of the region of interest. The surface integral on the right-hand side follows from application of the Gauss theorem (**n** is the normal vector of the surface). This term incorporates the boundary conditions (Neuman type) of the problem. The above form of the heat transfer problem is the natural starting point for the numerical solution using the Finite Element Method (FEM).

In the FEM solution, the problem is discretised with respect to the spatial co-ordinates. Here, the standard Galerkin approach is used [Zienkiewicz 1970]. First, the region of interest is divided to subsections with volumes Ω_e, the number of the elements being N_e ($e = 1, \ldots, N_e$). The geometrical partitioning is non-interlacing, *i.e.*, $\Omega = \bigcup_{e=1}^{Ne} \Omega_e$. The thickness of each element is $a_e = r_{e,2} - r_{e,1}$ and its dimension in the duct flow direction (z-direction) is Δl. Within the length Δl, the temperature is assumed to independent of the z co-ordinate.

Then the temperature field of each element is expressed using two functions with separated spatial and temporal dependence as $T_e^{(i)}(r,t) = \eta_e^{(i)}(r) \cdot T_e(t)$, $i = 1,2$. The spatial basis functions (the functions denoted as v in Eq. (3.12)) are chosen as $\eta_e^{(1)}(r) = \dfrac{r - r_{e,1}}{a^e}$ and $\eta_e^{(2)}(r) = 1 - \dfrac{r - r_{e,1}}{a^e}$.

Application of this procedure to the heat conduction problem produces the non-linear initial value problem

$$\mathbf{C}(t,T)\frac{d\mathbf{T}}{dt} + \mathbf{K}(t,\mathbf{T})\mathbf{T}(t) = \mathbf{f}(t,\mathbf{T}) \tag{3.13a}$$

with

$$\mathbf{T}(0) = \mathbf{T}_0 \quad \text{at } t = 0. \tag{3.13b}$$

Here, the vector **T***(t)* contains the calculated temperatures of the insulator at the positions of the spatial elements at time *t*, *i.e.* within the wall for each radial co-ordinate *r* which belongs to the element *e*

$$T_{ins}(r,t) = T_e(t)\,. \tag{3.14}$$

For radial co-ordinates corresponding to the duct inner or outer walls, the temperatures are determined by the boundary conditions. The dimension of **T** is $N_{nodes} \times 1$ where N_{nodes} equals $N_e + 1$.

The above equation (3.13a) is an ordinary non-linear differential equation system with a non-homogenous force term $\mathbf{f}(t,\mathbf{T})$ ($N_{nodes} \times 1$ vector) on the right-hand side. This factor, the capacity matrix **C** ($N_{nodes} \times N_{nodes}$) and the conductivity matrix **K** ($N_{nodes} \times N_{nodes}$) are assembled from the contributions of the elementary matrices as follows:

$$f^{(i)} = \left(f_e^{(1)}, f_e^{(2)}, f_e^{(3)}, \ldots, f_e^{(N_{nodes})}\right)^T \tag{3.15a}$$

where

$$f_e^{(i)} = 0 \text{ , if } 1 < i < N_{nodes} \tag{3.15b}$$

$$f_e^{(1)} = -2\pi\ \Delta l\ R_{in}\dot{q}''_{n,1} \tag{3.15c}$$

$$f_e^{(N_{nodes})} = -2\pi\Delta l R_{out}\dot{q}''_{n,2} \tag{3.15d}$$

and

$$\dot{q}''_{n,1} = -h_{in}\left(T_{gas} - T_{in}\right) - \varepsilon_{in}\sigma\left(T_{gas}^4 - T_{in}^4\right) \tag{3.15e}$$

$$\dot{q}''_{n,2} = -h_{out}\left(T_{\infty conv} - T_{out}\right) - \varepsilon_{in}\sigma\left(T_{\infty,rad}^4 - T_{ot}^4\right) \tag{3.15f}$$

The capacity matrix elements are

$$C^{(ij)} \equiv \sum_{e=1}^{N_e} C_e^{(ij)} \quad , i, j \ = 1, 2, \ldots, N_{nodes} \tag{3.16a}$$

where

$$C_e^{(ij)} = 2 \ \pi \ \Delta l \int_{r_{e,1}}^{r_{e,2}} \rho_{ins}\big(T(r)\big) \cdot C_{ins}\big(T(r)\big) \cdot \eta_e^{(i)} \cdot \eta_e^{(j)} \ rdr \tag{3.16b}$$

and

$$K^{(ij)} \equiv \sum_{e=1}^{N_e} K_e^{(ij)} \quad , i, j \ = 1, 2, \ldots, N_{nodes} \tag{3.17a}$$

where

$$K_e^{(ij)} = 2 \ \pi \ \Delta l \int_{r_{e,1}}^{r_{e,2}} k_{ins}\big(T(r)\big) \cdot \eta_e^{(i)} \cdot \eta_e^{(j)} \ rdr \ . \tag{3.17b}$$

The integrals for the conductivity matrix elements are performed numerically using the Gauss-Legendre integration scheme (one point method). For integrations required in evaluating the capacity matrices, the Newton-Cotes method (2-point method) was used in order to get diagonalised capacity matrices. The temporal integration of Eq. (3.13a) is performed by forward-Euler method,

$$\mathbf{T}(t_{n+1}) = \mathbf{T}(t_n) + \Delta t_{n+1} \ \mathbf{C}^{-1}(\mathbf{T}_n) \ \left(- \mathbf{K}(\mathbf{T}_n)\mathbf{T}_n + \mathbf{f}(t_n, \mathbf{T}_n) \right) \tag{3.18}$$

where the time steps are $\Delta t_{n+1} = t_{n+1} - t_n$.

As the temperature field inside the duct wall insulator, $T_{ins}(r,t)$, is solved (Eq. (3.14)), the duct wall temperature T_{in} required in Eq. (3.1) is obtained as the temperature of the insulator at its inner surface.

3.3 Solving the inverse problem: regularisation

From the SBI test, a time series of data readings $T_{data}(t_k)$ reflecting the thermocouple temperatures at the measuring times t_k are obtained. From the solution of the heat transfer problem described in the preceding sections, corresponding calculated values $T_{calc}(t_k, T_{gas}(t_k), \mathbf{a})$ are found. Here, the dependence of the calculated thermocouple temperatures on the unknown gas temperature values has been written explicitly in the

argument. Also the fact that the model is influenced by several other factors, such as the thermal properties of the duct wall, has been indicated by a vector **a**, which comprises the selected major factors. The determination of these factors is described in Appendix A.

If the parameters of vector **a** are known the least-squares solution of the problem of finding the time series $T_{gas}(t_k)$ means adjusting the values of $T_{gas}(t_k)$ at each time t_k so that the residual term

$$R = \sum_{k=1}^{M} \left(T_{calc}(t_k, T_{gas}(t_k), \mathbf{a}) - T_{data}(t_k) \right)^2 \tag{3.18}$$

is minimised. Here, *M* is the number data points included in the analysis. By employing interpolation between the data points, *M* may differ from the number of points collected in the SBI test.

In the present study the time series $T_{gas}(t_k)$ was presented using piece-wise linear functions which are continuous at their nodal points. The number *M* equals the number of the nodal points, which was chosen to be approximately 50, *i.e.*, clearly less than the 400 points collected in the SBI test.

As $T_{calc}(t_k, T_{gas}(t_k), \mathbf{a})$ and $T_{gas}(t_k)$ are related through the non-linear differential temporal differential equation (3.1) in which one of the parameters, T_{in}, is determined from a partial differential equation, finding physically meaningful set of values $T_{gas}(t_k)$ requires addition of auxiliary information to the minimisation scheme, *i.e.*, one has to solve the problem in regularised way [Tikhonov & Arsenin 1977, Groetsch 1993]. To get such a regularised solution of Eq. (3.18) we added a requirement that the solution should be as smooth as possible to the solution scheme. In the regularised form of Eq. (3.18) *R* must be minimised taking into account the constraint that the smoothness of $T_{gas}(t_k)$ should be maximised, *i.e.*, the absolute values of the numerically evaluated second derivative of $T_{gas}(t_k)$ should be as small as possible. Invoking the Lagrange's method of solving constrained minimisation problems using undetermined multipliers, the minimised term reads

$$R_\alpha = \sum_{k=1}^{M} \left(T_{calc}(t_k, T_{gas}(t_k), \mathbf{a}) - T_{data}(t\ ) \right)^2 + \alpha \sum_{k=1}^{M} \mathsf{S}\left\{ T_{gas}(t_k) \right\}^2 \tag{3.19}$$

where α is the Lagrange's multiplier or, the regularisation parameter, and $\mathsf{S}\left\{ T_{gas}(t_k) \right\}$ is a symbolic notation for the numerical second derivative operation. The basics of regularised solution of an inverse problem have been presented, e.g., in Press et al.

[1992] and examples of the use of the regularised least-squares method can be found in a publications of Myllymäki & Baroudi [1998, 2000].

There is considerable computational labour associated with finding the optimum value for the regularisation parameter α. To avoid this, we inverted the solution scheme of the problem as follows: the starting point of the procedure is to seek a solution, which fulfils the smoothness requirement imposed on the solution. In fulfilling this constraint the solution must, however, simultaneously satisfy the requirement that the least-squares residual should be sufficiently small. The quantitative measure to judge when the residual is sufficiently small is that there is no point in trying to force the residual below the noise level of the data, *i.e.*, the reduction of the residual may be stopped when this level is reached.

4. Evaluation of the heat loss terms

As the variety of specimen that can be tested in the SBI test is vast, any comprehensive estimates of the heat loss from the flames of the specimen to the specimen itself are to some extent uncertain and the mathematics becomes easily very tedious. When one considers the heat losses from the burner flames to the specimen, the situation is different: for the single device with well-defined operation instructions, rather general estimates of its behaviour may be established.

The determination of the losses of the heat convected from the main burner was based on temperature measurements by an IR camera on the cold side of the CaSi backing plate. The positions of the measuring points are shown in Figure 6. The data were collected when the backing plate temperatures had reached a stationary state. Three tests were made: two with the burner nominal heat output set to 30 kW and one with 60 kW setting.

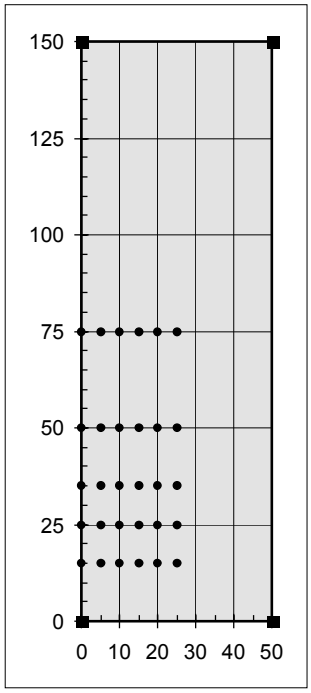

Figure 6. The positions of the IR camera measurement points. The circles depict the measurement points and the squares indicate places at which temperature readings were collected mainly for checking purposes.

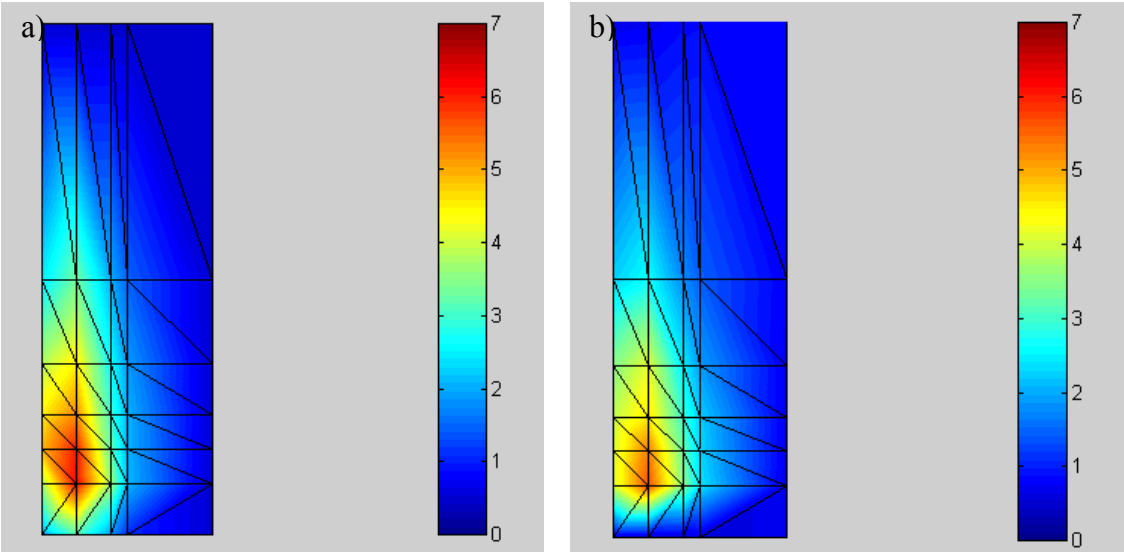

Figure 7. The heat fluxes determined from the temperatures measured with the IR camera. The nominal heat release of the main burner was 30 kW in both tests. The calculated total amounts of heat absorbed are the following: for the whole backing plate they are 1.31 kW (a) and 1.28 kW (b) and for the effective area 0.43 kW (a) and 0.38 kW (b). The different colours correspond to different heat fluxes in kW/m^2.

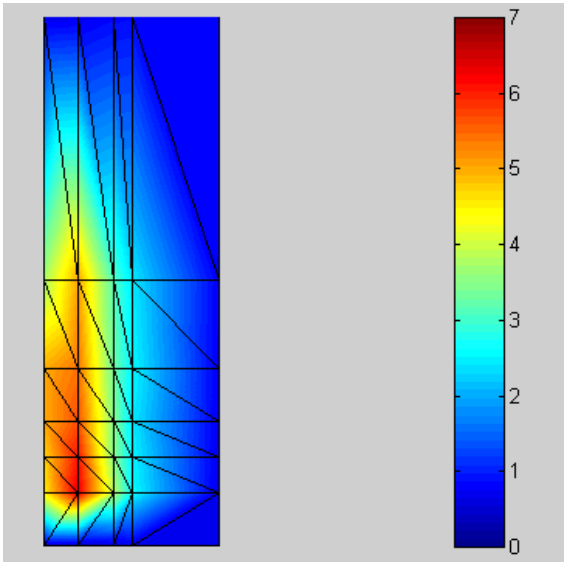

Figure 8. The heat fluxes determined from the temperatures measured with the IR camera. The nominal heat release of the main burner was 60 kW. The calculated total amounts of heat absorbed are 1.68 kW for the whole backing plate and 0.84 kW for the effective area. The different colours correspond to different heat fluxes in kW/m^2.

The temperature readings were converted to heat flux $\dot{q}''_{bp}$ emitted by the backing via the formula

$$\dot{q}''_{bp} = h_{bp,out}\left(T_{bp} - T_{amb}\right) + \varepsilon_{bp}\sigma\left(T_{bp}^4 - T_{amb}^4\right), \quad (4.1)$$

where T_{bp} are measured temperatures. The other parameters are the heat transfer coefficient of the outer face of the backing plate ($h_{bp,out}$ = 10 kW/m^2), its emissivity (ε_{bp} = 0.7) and the ambient temperature (T_{amb} = 20 °C). The heat fluxes obtained in the three tests are shown in Figure 7and Figure 8.

From the heat flux mappings, an effective area, A_{eff}, was estimated through which the major part of the heat transfer occurs, see Figure 9. The heat flux distributions were also integrated over the whole plate to get an estimate on the magnitude of the total heating power Q_{bp} exposed to the backing plate. The ratio of Q_{bp} to A_{eff} was taken to represent an effective heat flux value characteristic SBI main burner. The results are summarised in Table 2.

The results based on the outer surface temperature readings were checked by comparing them to results obtained through another approach. For this approach, two thermocouples were embedded into the CaSi board, one close to the hot surface and the other in the middle way between the inner and outer faces of the board. The readings from these thermocouples were then analysed using the methods described in Chapter 3 (Figure 10a). For this analysis, the cylindrical geometry of the duct calculations was transformed to a planar geometry by assigning large values to the radii of the inner and outer wall. At steady state, the calculated value was 4.0 kW/m^2, which is the same as the value of ca. 4 W/m^2 obtained via the IR camera measurements (Figure 10b).

As a result of this inquiry we evaluated the heat loss to the specimen from the main burner, *i.e.*, the term $Q_{loss,specimen,main}$ of the model given in Chapter 2 with the following method. First, the heat flux value was calculated using data on the thermal properties of the specimen. Then, the heat loss rate was evaluated by multiplying this heat flux value with the effective area corresponding to the burner heat output (0.0975 m^2 for the normal SBI test output of 30 kW).

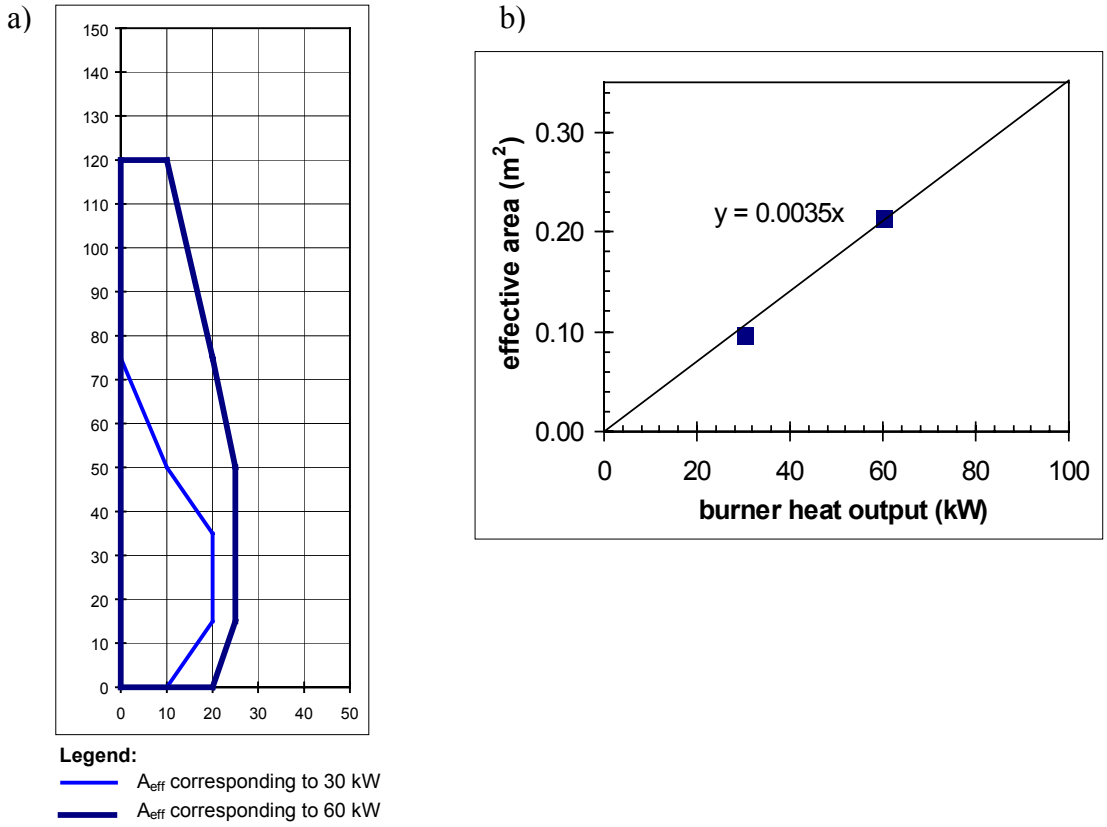

Figure 9. a) The effective heat-transfer areas for the main burner nominal heat output of 30 kW and 60 kW. For 30 kW, $A_{eff} = 0.0975\ m^2$ and for 60 kW, $A_{eff} = 0.2150\ m^2$. b) Graph enabling extrapolations or interpolations to other burner heat output values.

Table 2. The effective area, total heating power and the effective heat flux.

burner heat output (kW)	**total heat delivered to the backing plate (kW)**	**effective area (m^2)**	**total heat delivered to the effective area (kW)**	**effective heat flux (kW/m^2)**
30	1.31	0.0975	0.432	4.43
30	1.28	0.0975	0.376	3.88
60	1.68	0.2150	0.843	3.92

a)

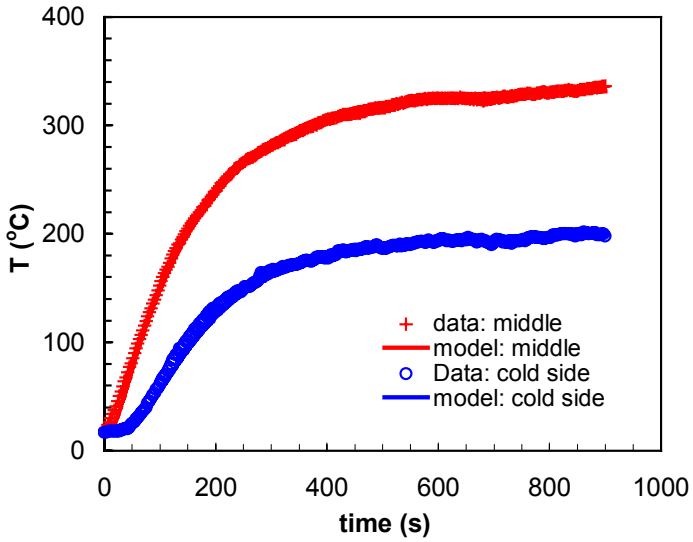

b)

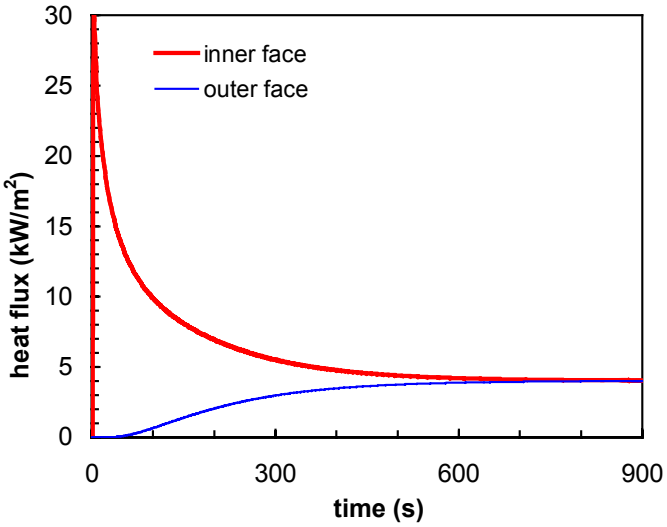

Figure 10. a) The temperatures measured inside the backing plate and the predictions for the data obtained using the calculation scheme described in Chapter 3. b) The heat fluxes derived from the calculated temperatures are shown in Fig. b. The heat flux values of the inner (hot) and outer (cold) faces of the backing plate converge to 4.0 kW/m^2.

5. Application of the method to analyse some SBI RR data

The performance and implications of the analysis method were inspected by applying the method to four tests done in the SBI Round Robin at VTT. The products tested in these experiments were 1) product M19, unfaced Rockwool, 2) product M05, varnished pine timber, 3) product M03, fire-retarded extruded polystyrene (FR EPS) board and 4) product 30, paper-faced glass wool.

Product M19 was selected since it had the lowest heat production of all the SBI RR products. Material M05 represents a wooden construction product. The FR EPS board was chosen to represent a material with high heat generation rate. In the experiment with product M30, the heat was released by the paper sheet in a short period of time. The material parameters used in estimation of the heat losses for each product are given in Table 3. The heat transfer coefficients for the inner and outer surfaces of the specimen were 27 kW/m^2 and 12 kW/m^2, respectively[†].

Table 3. The parameters used to characterise the thermal behaviour of the specimens.

quantity	**M19 unfaced Rockwool**	**M05 varnished pine timber**	**M03 FR EPS board**	**M30 paper-faced glass wool**[**)]
thickness (mm)	50	10	40	100
density (kgm^{-3})	140	380	32	18
thermal conductivity (WK^{-1}m^{-1})	0.036[*)]	0.14	0.032	0.020
specific heat (Jkg^{-1}K^{-1})	800	400	1200	800

*) Value at room temperature. In the calculations, the temperature dependence of thermal conductivity was taken into account.

**) Values of the glass wool.

[†] The value 12 kW/m^2 is slightly larger than the value of 10 kW/m^2 mentioned in Chapter 4. It was established by studying the data in more details using the regularised least-squares method.

5.1 Temperatures

The results of the regularised least-squares fitting procedure are shown in Figure 11, Figure 12, Figure 13 and Figure 14. In these figures, there are shown the measured data, the calculated prediction for the data and the gas temperatures which correspond to the calculated thermocouple values.

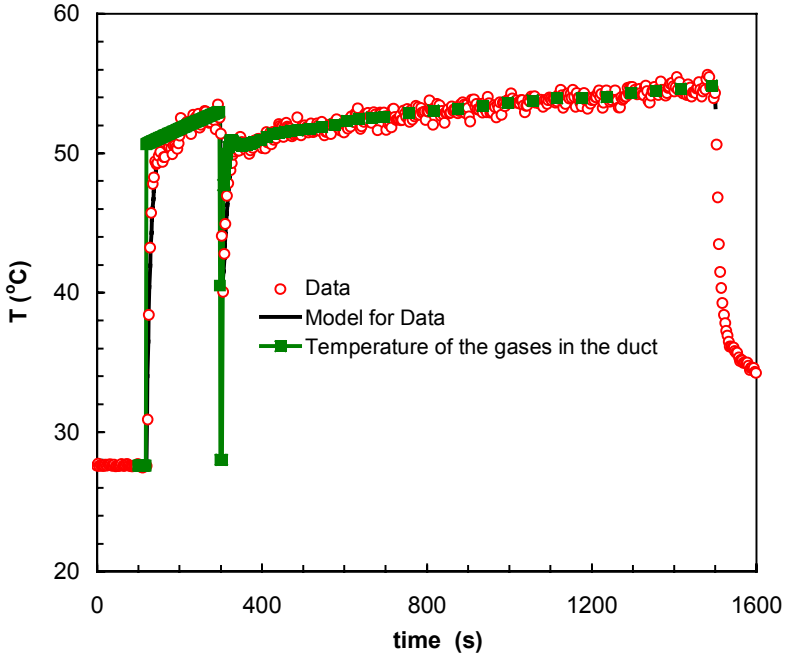

Figure 11. SBI Round Robin material M19 (Rockwool): measured temperature data, the calculated prediction for it and the corresponding gas temperature.

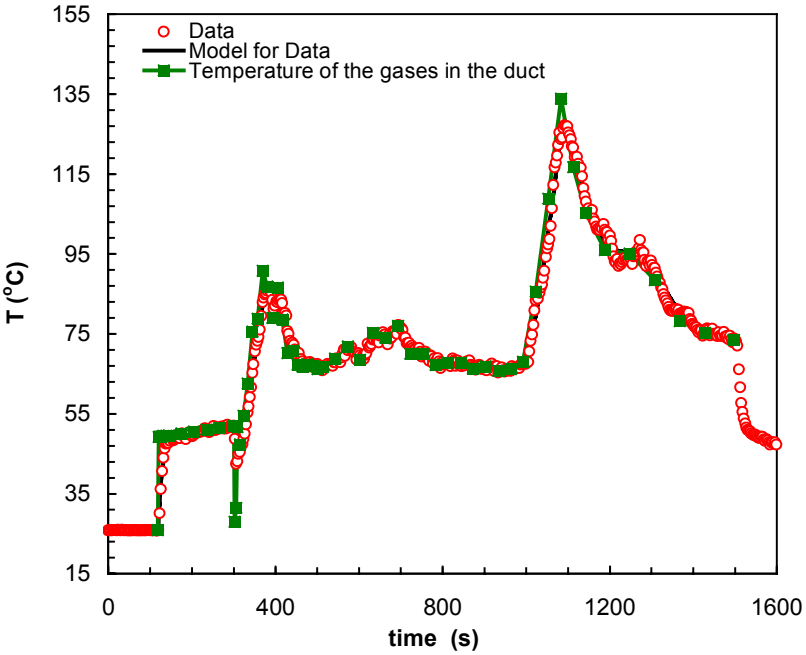

Figure 12. SBI Round Robin material M05 (varnished pine timber): measured temperature data, the calculated prediction for it and the corresponding gas temperature.

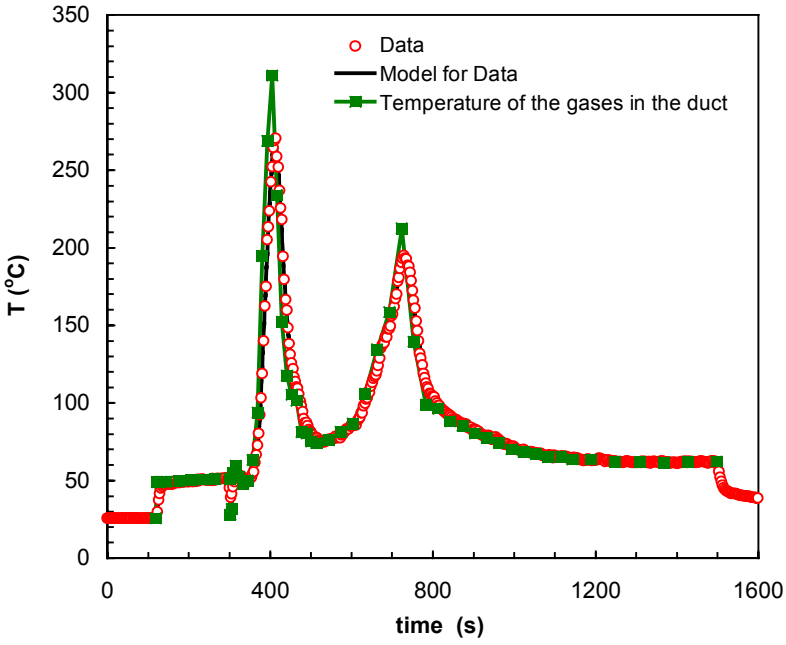

Figure 13. SBI Round Robin material M03 (FR EPS board): measured temperature data, the calculated prediction for it and the corresponding gas temperature.

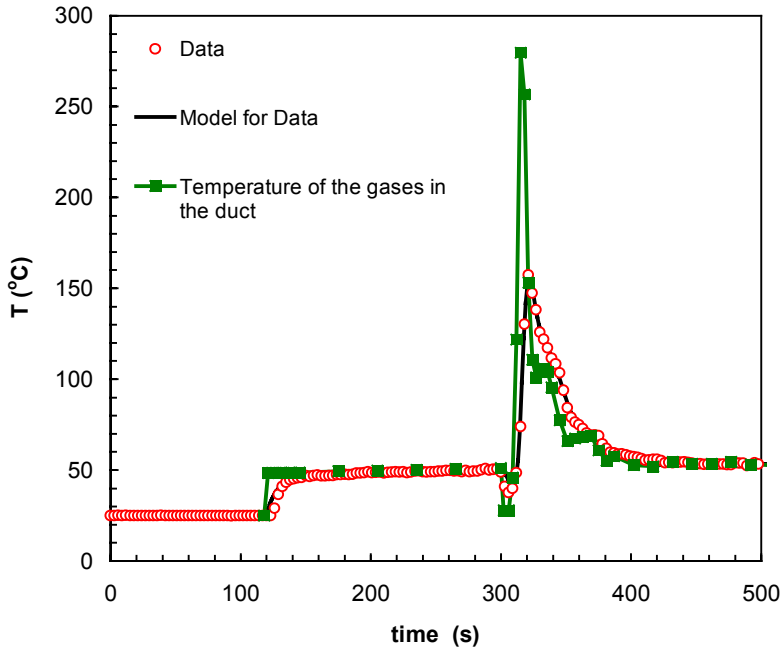

Figure 14. SBI Round Robin material M30 (paper on glass wool): measured temperature data, the calculated prediction for it and the corresponding gas temperature.

It may be seen that changes in the gas temperature are more rapid than the changes in the measured temperatures. Also the temperature of the gases in duct is higher than the measured values. Both these phenomena are most pronounced in the early phases of the test. Towards the end of the test, the temperature of the measuring element approaches the gas temperature. Also the lower the temperatures in the test are, the more faithfully the temperature measurements reveal the temperature prevailing in the duct. For the product M19 which did not release heat practically at all, the gas temperatures and the measured values are within the experimental noise for the SBI test starting at ca. 300 s. In the case of product M30 with a fast rise to a relatively high heat release rate, the difference between the gas temperature and the thermocouple reading rises as high as 90 °C. For M03 the maximum difference was *ca.* 40 °C and for M05 *ca.* 10 °C.

5.2 Convective rate of heat release of the specimen

The values of the convective portion of the rate of heat release of the specimens are shown in Figure 15, Figure 16, Figure 17 and Figure 18.

For comparison, also predictions for this quantity derived via a rudimentary way directly from the measured data are depicted. These values are obtained by first multiplying the measured ΔT by the density, specific heat and flow rate of the gases in

the duct and then subtracting from this value the convective heat released by the auxiliary burner at the end of its burning period (an average between 250 s and 290 s).

The two approaches may be compared through a quantity resembling the fire-growth index used in the evaluation of the results of the SBI test (Table 4). Here, the index we use is obtained by diving the maximum value of the convective rate of heat release by the time required to reach that value with the zero moment set at 300 s. It is seen that the delay and loss of magnitude in the measured ΔT values reduce the index values considerably.

Table 4. Ratio of the first maximum of the convected RHR to the time elapsed from 300 s to the time of the maximum in W/s.

analysis method	**M05 varnished pine timber**	**M03 FR EPS board**	**M30 paper-faced glass wool**
method developed in this study	430	1450	7580
directly from the measured ΔT	260	1020	2940

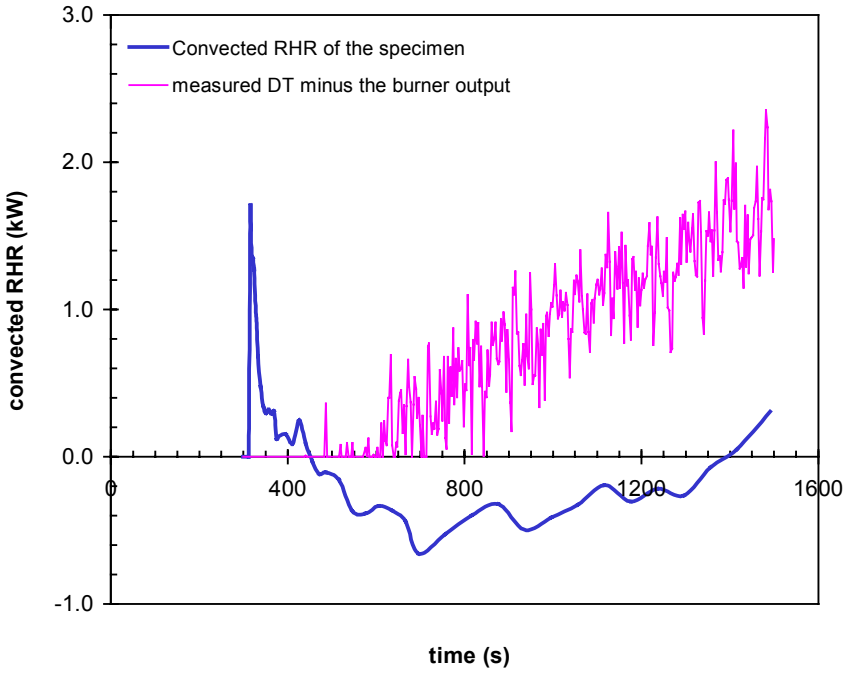

Figure 15. Convective heat released by the SBI Round Robin material M19 (unfaced Rockwool): the thick curve represents the output of the analysis of this study and the thin curve a prediction of a rudimentary approach utilising the measured ΔT values.

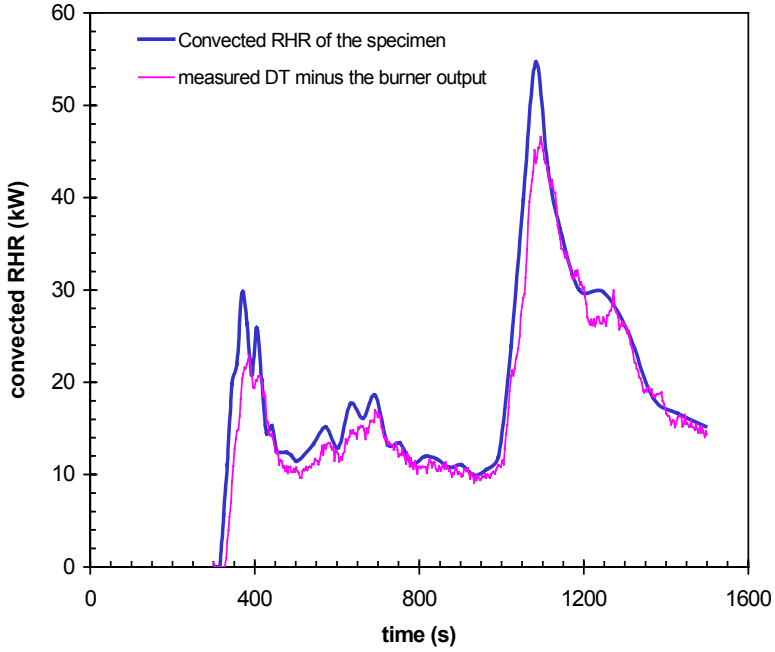

Figure 16. Convective heat released by the SBI Round Robin material M05 varnished pine timber): the thick curve represents the output of the analysis of this study and the thin curve a prediction of a rudimentary approach utilising the measured ΔT values.

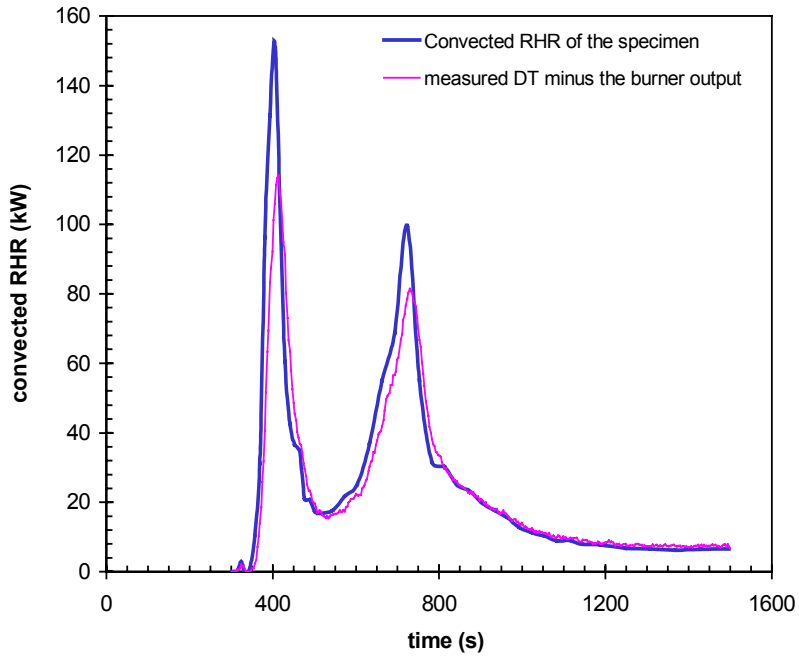

Figure 17. Convective heat released by the SBI Round Robin material M03 (FR EPS board): the thick curve represents the output of the analysis of this study and the thin curve a prediction of a rudimentary approach utilising the measured ΔT values.

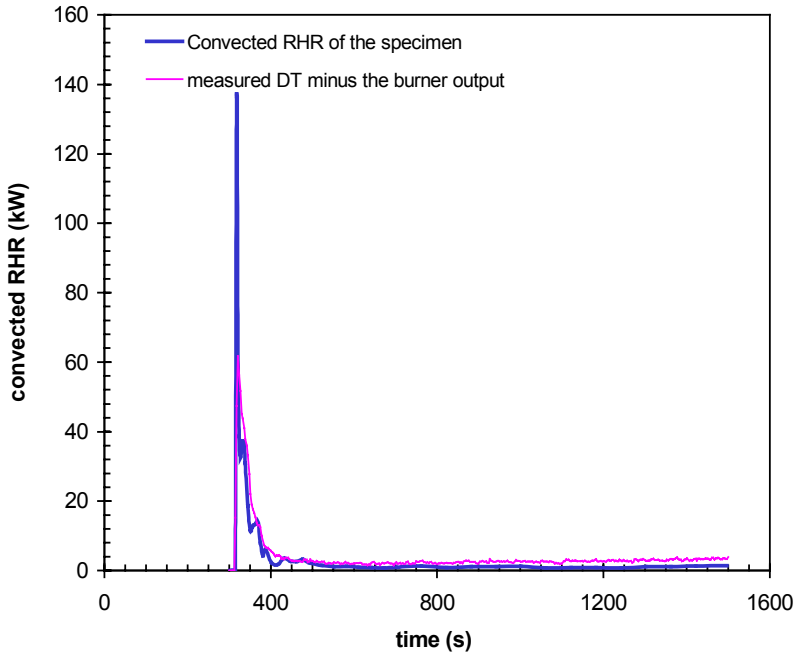

Figure 18. Convective heat released by the SBI Round Robin material M30 (paper-faced glass wool): the thick curve represents the output of the analysis of this study and the thin curve a prediction of a rudimentary approach utilising the measured ΔT values.

5.3 Estimations on the total rate of heat release of the specimen

The convective portion of the rate of heat release can be converted to the total or, in other words, chemical rate of heat release provided that the partitioning of the heat release rate to its convective and radiative fractions is known. For many building materials these fractions are known at least approximately but for many materials such information is not readily available. For some materials, *e.g.* wood, the situation complicated by the fact the convective and radiative fractions are not constant through the whole test but change as the material is modified during burning.

An inclusion of radiation measurement sensors to the SBI test apparatus would in principle enable determination of the amount of radiated heat. In practise this task is, however, rather cumbersome and prone to errors in the experiments and data analysis. The possibility of converting the convective RHR value total RHR through radiation measurements was addressed in this study. While some of the results were generally in agreement with known results (*e.g.* for propane, the measured radiative fraction was approximately between 25 % and 30 %), deviations due to small, in practise

unavoidable, changes in the measuring configuration and the noise in the radiation data render this approach unsuitable for practical purposes.

Naturally, the SBI RR data that was analysed in this study included the total RHR values obtained by the oxygen-depletion calorimetry. By comparing the convective RHR data of Figure 15-Figure 18 to the total RHR values, one may estimate the convective fraction of the products. Results of such an exercise are shown in Figure 19, Figure 20 and Figure 21, where the convective fraction was allowed to change linearly during the experiment. The results for convective fractions of the analysed materials are the following: 61 % - 70 % for M05, 49 % - 87 % for M03 and 80 % for M30. Graphically the results are shown in Figs. 5.9-5.11.

For product M30 an estimate for the total heat released (THR) by the specimen may readily be estimated since its major contribution comes from the paper which burner out almost completely. As described in Appendix B, an estimate of 4 MJ may be obtained for THR which includes also the contributions from the wool binder substances. By integrating the RHR curves of Fig. 5.11, the RHR values obtained using the oxygen-depletion method give a value of THR = 13.5 MJ and the RHR estimate of the present analysis yields a value THR = 3.9 MJ which is in excellent agreement with the value THR estimate of 4 MJ.

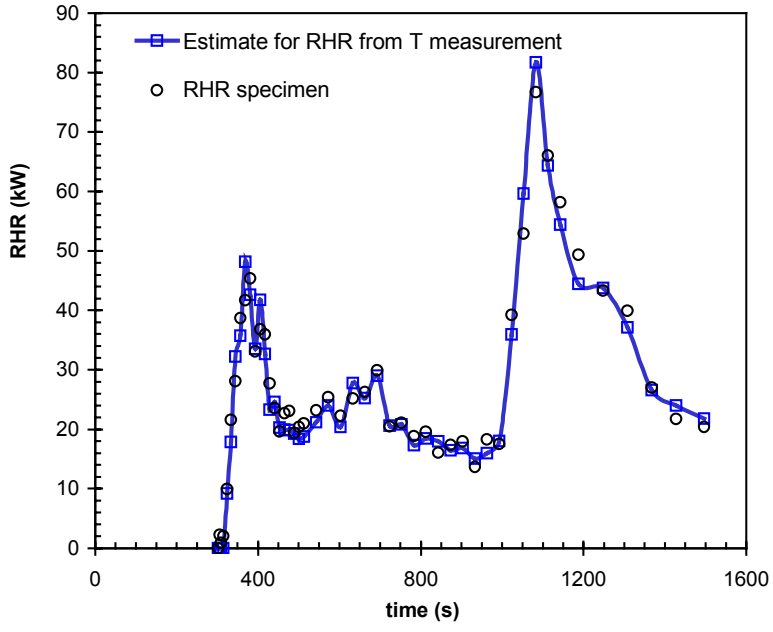

Figure 19. Material M05: the total heat release obtained from the convective heat release by dividing by a convective fraction changing linearly from 61 % to 70 % during the test (thick curve). The RHR values determined by the oxygen-depletion technique are shown by the empty circles.

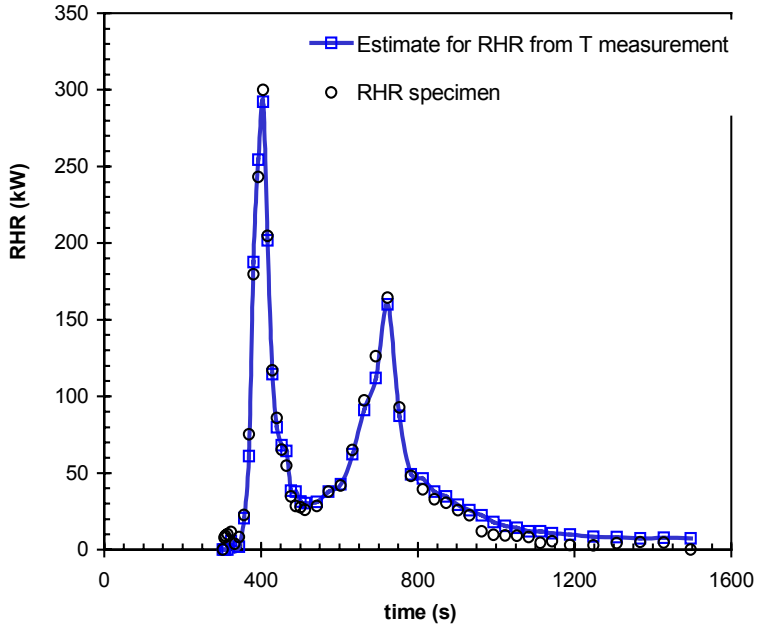

Figure 20. Material M03: the total heat release obtained from the convective heat release by dividing by a convective fraction changing linearly from 49 % to 87 % during the test (thick curve). The RHR values determined by the oxygen-depletion technique are shown by the empty circles.

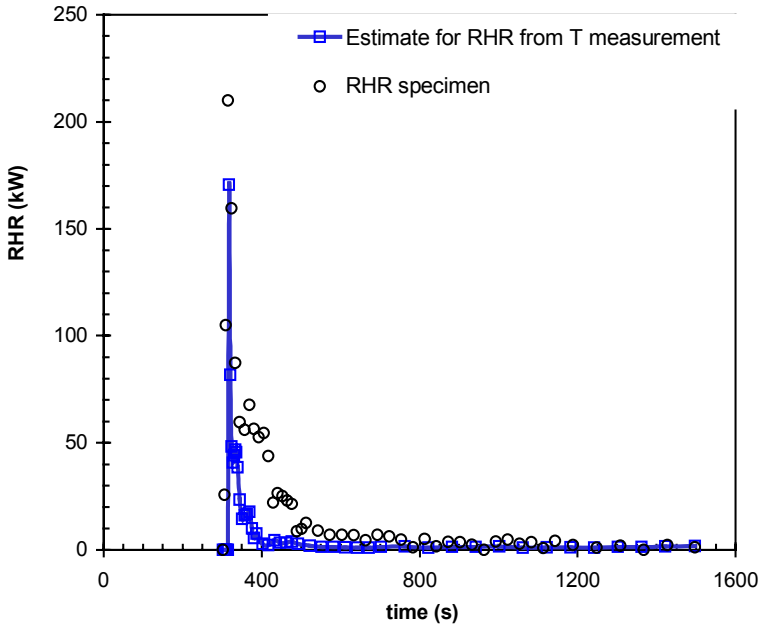

Figure 21. Material M30: the total heat release obtained from the convective heat release by dividing by a convective fraction equal to 80 % (thick curve). The RHR values determined by the oxygen-depletion technique are shown by the empty circles.

6. Summary and concluding remarks

In the SBI fire test, there are temperature sensors in the exhaust duct allowing measurement of the temperature rise of the exhaust gases (ΔT measurement). In principle these sensors provide means to monitor the production rate of thermal energy. However, while traversing to the exhaust duct the heated gases lose energy to their surroundings which in a rigorous determination of the heat release rate of the specimen must be taken into account. Thus, the experimentally simple ΔT approach for rate-of-heat-release evaluation requires a very complex data analysis with inherently high uncertainty and proneness to systematic errors. Thus the method is not suitable for routine testing and classification purposes.

However, for less demanding applications, such as quality control and product development purposes the ΔT can in some cases provide a well-suited option for RHR assessment. The method can also be used in fire research, e.g., to analyse the convective portion of the total heat release.

This study addresses the problem of interpreting of the measured temperatures in terms of physically relevant quantities, *i.e.*, the rate of heat release. The analysis produces straightforwardly the convective part of RHR of the specimen. From this value, also the total heat released may be inferred if there is information available on the partitioning of the RHR to its convective and radiative portions. While such information is readily obtainable for basic building construction materials, for majority of the new products developed in industry, the data may be missing or incomplete and precarious extrapolations from the existing data to the new cases may be necessary.

The temperature analysis method developed in this study is based on a simplified model of the heat transfer in the SBI system and a mathematical formulation to describe this system. Experiments were carried out to check the operation of the calculation codes and to establish and verify the heat transfer model.

The solution of the problem entails handling of an inverse heat-transfer problem. The novelty of the presented solution lies in the use of the regularised output least-squares method to tackle with this problem. The dextrous numerical solution of developed enables execution of the whole analysis by a spreadsheet program (EXCEL).

The analysis comprises the following steps: 1) data retrieval from the SBI data files and their pre-processing, 2) solving the heat flow rate in the exhaust duct from the ΔT data, 3) calculations to predict the major heat loss terms and 4) combination of the results to the final results. As majority of the operations can be executed automatically by EXCEL

Macros, integration of the program into, e.g., the SBI data-analysis software is straightforward.

Besides the SBI apparatus, the temperature data analysis method developed in this study could in principle be applied also in other fire test set-ups. The calculations of the problem are already rather compact, but through further refinement of the user interface, this part of the problem solving could readily be made accessible to wider range of users within the fire-safety practisers. The problems associated with the estimation of the heat losses could be alleviated by establishing a large database with detailed data on thermal properties of materials.

Acknowledgements

The financially support from Nordtest is gratefully acknowledged.

The authors thank Mr. K. Taimisalo and Mrs. T. Hakkarainen for their contributions to the experimental work and Mr. J. Myllymäki for the several ideas he so kindly shared with us concerning the practical procedures of solving the mathematical problems. Dr. M. Kokkala and Dr. E. Mikkola are acknowledged for reviewing and revising the manuscript.

References

Babrauskas, V. 1997. Tables and Charts. In: Fire Protection Handbook. 18th ed. Quincy: National Fire Protection Association. ISBN 0-87765-377-1

Groetsch, C. W. 1993. Inverse Problems in the Mathematical Sciences. Vieweg: Wieweg Mathematics for Scientists and Engineers. 151 p.

Myllymäki, J. and Baroudi, D. 1998. Determination of Thermal Properties. Applications of Regularized Output Least-Squares Method. Espoo: The Technical Research Centre of Finland. 54 p. (VTT Publications 351.) ISBN 951-38-5239-3

Myllymäki, J. & Baroudi, D. 2000. A method to determine thermal conductivity using boundary temperature measurements. Poitiers: Proceedings of the 6th International Symposium. 5–9 July 1999. International Association for Fire Safety Science. Pp. 349-360. ISBN 0-925-223-25-5

Parker W.J. 1984. Calculations of the Heat Release Rate by Oxygen Consumption for Various Applications. Journal of Fire Sciences, Vol. 2, No. 5, pp. 380–395.

Press, W. H., Teukolsky, S. A., Vetterling, W. T. & Flannery, B. P. 1992. Numerical Recipes In FORTRAN. The Art of Scientific Computing. 2dn Edition. New York: Cambridge University Press. 963 p.

Tewarson, A. 1995. Generation of Heat and Chemical Compounds in Fires. In: SFPE Handbook of Fire Protection Engineer-ing. 2nd ed. Quincy: National Fire Protection Association. ISBN 0-87765-353-2

Tikhonov, A. N. & Arsenin, V. Y. 1977. Solutions of Ill-Posed Problems. Wiley: New York. 87 p.

Vandevelde, P. 1980. An Evaluation of Heat Release Criteria in Reaction-to-Fire Tests. Fire and Materials, Vol. 4, No. 3, pp. 157–162.

Zienkiewicz, O. C. 1970. The Finite Element Method in Engineering Science. London: McGraw-Hill. 521 p.

Appendix A: Determination of the factors influencing temperature measurements

The relation between the calculated gas and thermocouple temperatures depends on the temperature of the inner wall of the exhaust duct wall or, via this quantity on the thermal properties of the duct wall insulation. The factors which were determined experimentally are the density ρ_{ins}, thermal conductivity k_{ins} and specific heat C_{ins} of the insulator. Other factors describing the duct wall, such as the properties of the metal sheets inside and outside of the insulator were taken from literature and the construction details of the SBI apparatus.

Also all heat transfer coefficients are unknown and were determined experimentally. These are the heat transfer coefficient of the thermocouple surface h_c, and the heat transfer coefficients h_{in} and h_{out} of the duct's inner and outer surfaces, respectively. The symbolic vector **a** in section 3.3 comprises the above mentioned parameters. Below we refer to them by a term "system parameters".

The parameters were determined from temperature data measured in the duct and on its outer surface. The data collected from three tests, two performed using nominal burner output of 30 kW and one with 60 kW output.

The study proceeded through iterations, *i.e.*, first we assigned to the system parameters values obtained from literature and performed the least-squares fitting by changing the gas temperature values. The next run was made by keeping the gas temperatures constant and letting the system parameters be adjustable. These two operations were repeated until both the gas temperature and the system parameters converged to values which did not change in further iterations. The values obtained form the system parameters are given in Table A1.

Table A1. The parameters used in the calculations described in Chapter 3.

parameter	**value**
$C_{ins} \cdot \rho_{ins}$	175 $kJK^{-1}kg^{-1}$
$k_{ins} = k_0 \cdot \left(1 + \left(\frac{T}{411\ \mathrm{K}}\right)^{2.404}\right)$, with k_0 =	0.074 $WK^{-1}m^{-1}$
h_c	251 $WK^{-1}m^{-2}$
h_{in}	26.6 $WK^{-1}m^{-2}$
h_{out}	6.9 $WK^{-1}m^{-2}$

Note: the above formula for the temperature dependence of the thermal conductivity of the insulator was obtained by analysing the data supplied by the manufacturer.

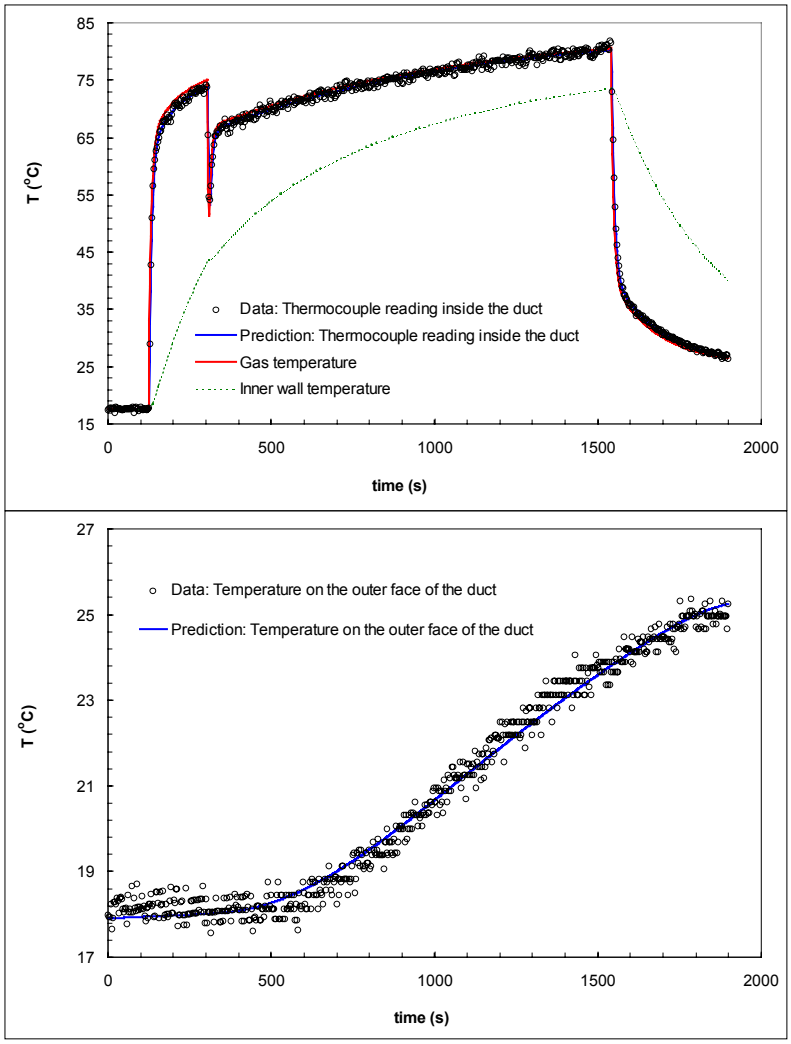

Figure A1. Results of an experiment to determine the system parameters affecting the temperature measurement in the SBI system: a) the measured data, its predicted value, the gas temperature as well as the duct wall temperature and b) temperatures measured on the outer face of the duct together with a calculated prediction for them. The timing of the test differed from the SBI test partially to get more data values and partially because simultaneously IR camera readings were collected on the cold side on the backing plate.

Appendix B: On the contributions of paper and glass wool to the heat released by the SBI Round Robin product M30

Product M30 of the SBI Round Robin consist of a paper fixed on a glass wool backing. The surface density of the paper is 90 g/m^2 and the thickness and density of the wool are 100 mm and 18 kg/m^3, respectively. The area of specimen's surface is 2.25 m^2.

The estimation of the total heat released (THR) by the paper is straightforward as the paper may be assumed to have burned off completely. If we assign a value of 15 MJ/kg for the heat combustion of paper, we obtain an estimate of $THR_{paper} = 3$ MJ for the paper contribution.

For glass-wool contribution an estimate of $THR_{wool} = 1$ MJ is used. The evaluation of the heat evolving from the glass wool was made using two approaches: firstly, from cone calorimeter experiment results and secondly, by approximate calculation.

The cone calorimeter tests were made for two samples, one consisting of the M30 paper only and the other including also the glass wool. The heat release rate values per unit sample area obtained in these two tests are shown in Figure B1. From the data it is seen that the sample made of paper and wool produced more heat than the sample made of paper. The difference, 0.34 MJ/m^2, gives an estimate for the THR per unit sample area of the glass wool. Using the SBI sample area of 2.25 m^2, this may be converted an estimate of the total heat released by the glass wool in the SBI test, $THR_{wool,cc} = 0.8$ MJ.

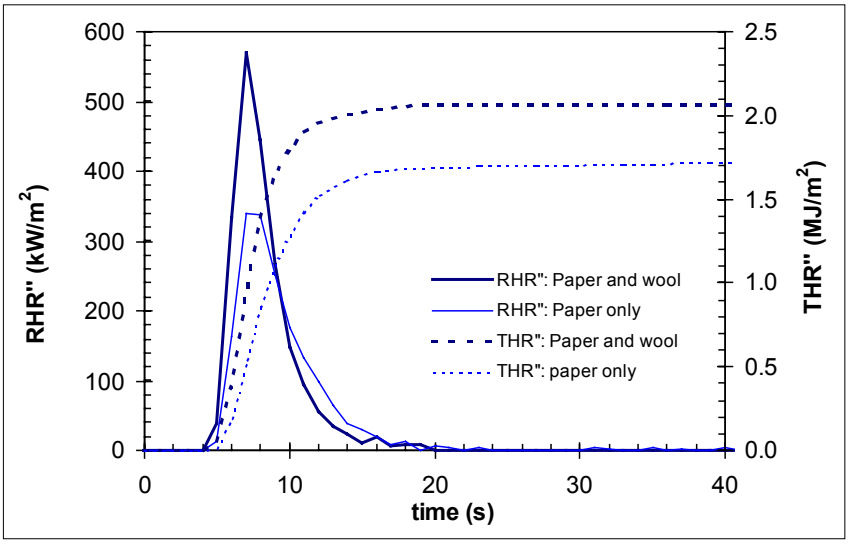

Figure B1. Cone calorimeter data on product M30: Rate of heat release (solid curves) and total heat released (dashed curves) per unit sample area of a paper sample (thinner curves) and a sample made of paper glass wool (thicker curves).

The heat evolved from the glass wool may be estimated also through physical characteristics and the size of the piece of wool involved in the burning process. First, we assume that the wool may be considered as two parts with different sizes and damage penetration depths.

The portion of wool directly affected by the main burner through the whole test has been assumed to have a damage depth equal to the thickness of the wool, *i.e.*, 100 mm. Its area is assumed to consist of two stripes of width of 0.20 m and height of 1.50 m, *i.e.*, the total area is 0.60 m^2. Using the density of the wool of *ca.* 20 kg/m^3, an estimate for the mass this portion of the wool is 1.2 kg.

The rest of the glass wool is affected primarily only by the short-time heat release exposure from the burning paper and, thus, the thickness of damaged area is rather small. We assign it a value of 1 cm obtained from the cone calorimeter experiments. As the area is *ca.* 1.65 m^2, the mass of this part of the wool is 0.33 kg.

The characteristics of the binder substances in the glass wool may assumed to resemble those of different sorts of oils. Thus, we may assume that their heat of combustion is in the range of ca. 20 to 40 MJ/kg. The binder content varies considerably in different glass wool products. A typical binder content for a glass wool with density of 100 kg/m^3 is *ca.* 10 %. For the wool of M30 with density of 20 kg/m^3 the binder content is presumably less than 10 %, *e.g.*, 2 %. Using the value of 30 MJ/kg of heat of combustion and 2 % for the binder content, the calculated estimate for the total heat released by the glass wool in the SBI test reads $THR_{wool,calc}$ = 1 MJ, which is close to the estimate obtained from the cone calorimeter experiments.

Published by

Vuorimiehentie 5, P.O.Box 2000, FIN–02044 VTT, Finland
Phone internat. +358 9 4561
Fax +358 9 456 4374

Series title, number and report code of publication

VTT Research Notes 2136
VTT–TIED–2136

Author(s)
Hietaniemi Jukka & Baroudi, Djebar

Title

Physical Interpretation of Temperature Data Measured in the SBI Fire Test

Nordtest Technical Report 416

Abstract

In the SBI fire test, there are temperature sensors in the exhaust duct allowing measurement of the temperature rise of the exhaust gases (ΔT measurement). In principle these sensors provide means to monitor the production rate of thermal energy. However, while traversing to the exhaust duct the heated gases lose energy to their surroundings which in a rigorous determination of the heat release rate of the specimen must be taken into account. There is also another factor hampering the conversion of the ΔT values to the thermal energy readings, namely the fact that the temperature readings do not directly show the temperature of the gases, but rather reflect it through a heat transfer process involving also the duct wall temperatures. These complications make the experimentally simple approach to use ΔT for rate-of-heat-release evaluation a complex task with inherently high uncertainty and proneness to systematic errors. Thus the method is not suitable for routine testing and classification purposes.

However, for some other applications, such as quality control and product development purposes, the ΔT method can in some cases provide a well-suited option for RHR assessment. The method can also be used in fire research, e.g., to analyse the convective portion of the total heat release.

In this report we present a method to interpret the ΔT values in terms of physically relevant factors describing generation and loss of heat. The analysis yields straightforwardly the convective part of RHR of the specimen. However, to evaluate the total RHR of the specimen, external sources of information must be exploited to establish the radiative contribution of the total RHR.

The analysis method is based on a simplified model of heat transfer in the SBI system and its mathematical formulation. The solution of the problem entails handling of an inverse heat-transfer problem. The novelty of the presented solution lies in the use of the regularised output least-squares method to tackle with this problem. The dextrous numerical solution of developed enables execution of the whole analysis by a spreadsheet program (EXCEL). As majority of the operations can be executed automatically by EXCEL Macros, integration of the program into, e.g., the SBI data-analysis software is straightforward.

Experiments were carried out to establish and verify the heat transfer model and to check the operation of the calculation codes.

Besides the use in connection with the SBI apparatus, the data analysis method developed in this study can in principle be applied also in other fire tests.

Keywords
fire tests, fire protection, SBI, temperature measurement, data analysis, exhaust gases, heat transfer

Activity unit
VTT Building and Transport, Kivimiehentie 4, P.O.Box 1803, FIN–02044 VTT, Finland

ISBN	Project number
951–38–5958–4 (soft back ed.) 951–38–5959–2 (URL: http://www.inf.vtt.fi/pdf/)	R2SU00391

Date	Language	Pages	Price
April 2002	English	47 p. + app. 4 p.	B

Name of project	Commissioned by
Physical Interpretation of Temperature Data Measured in the SBI Fire Test (Nordtest project no. 1381-98)	Nordtest, VTT Building and Transport

Series title and ISSN	Sold by
VTT Tiedotteita – Research Notes 1235–0605 (soft back edition) 1455–0865 (URL: http://www.inf.vtt.fi/pdf/)	VTT Information Service P.O.Box 2000, FIN–02044 VTT, Finland Phone internat. +358 9 456 4404 Fax +358 9 456 4374